iScience

CellPress
OPEN ACCESS

Article

GL-V9 inhibits the activation of AR-AKT-HK2 signaling networks and induces prostate cancer cell apoptosis through mitochondria-mediated mechanism

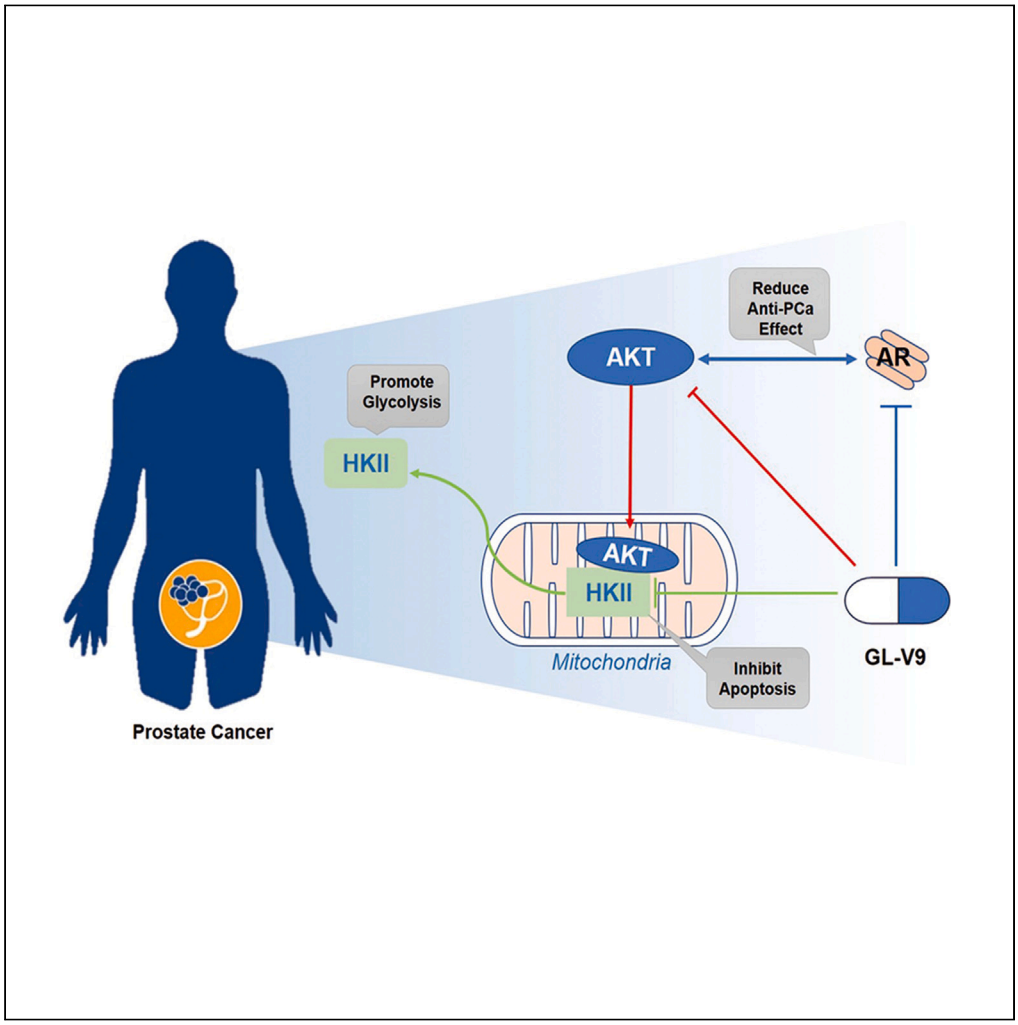

Rui Wang, Qi Min, Yongjian Guo, ..., Dechao Wang, Yuan Gao, Libin Wei

435204445@qq.com (Y.G.)
wlbiws_1986@aliyun.com (L.W.)

Highlights

GL-V9 induces mitochondria-mediated apoptosis in AR-positive and AR-negative PCa cells

GL-V9 suppresses *p*-AKT, mitochondrial location of HKII and activation of AR signal

GL-V9 disrupts feedback activation of AKT signaling in condition of AR inhibition

GL-V9 exhibits a synergistic effect when combined with AR inhibitors in PCa treatment

Wang et al., iScience *27*, 109246
March 15, 2024 © 2024 The Author(s).
https://doi.org/10.1016/j.isci.2024.109246

iScience

CellPress
OPEN ACCESS

Article

GL-V9 inhibits the activation of AR-AKT-HK2 signaling networks and induces prostate cancer cell apoptosis through mitochondria-mediated mechanism

Rui Wang,[1,5] Qi Min,[3,4,5] Yongjian Guo,[1] Yuxin Zhou,[1] Xin Zhang,[1] Dechao Wang,[1] Yuan Gao,[2,*] and Libin Wei[1,6,*]

SUMMARY

Prostate cancer (PCa) is a serious health concern for men due to its high incidence and mortality rate. The first therapy typically adopted is androgen deprivation therapy (ADT). However, patient response to ADT varies, and 20–30% of PCa cases develop into castration-resistant prostate cancer (CRPC). This article investigates the anti-PCa effect of a drug candidate named GL-V9 and highlights the significant mechanism involving the AKT-hexokinase II (HKII) pathway. In both androgen receptor (AR)-expressing 22RV1 cells and AR-negative PC3 cells, GL-V9 suppressed phosphorylated AKT and mitochondrial location of HKII. This led to glycolytic inhibition and mitochondrial pathway-mediated apoptosis. Additionally, GL-V9 inhibited AR activity in 22RV1 cells and disrupted the feedback activation of AKT signaling in condition of AR inhibition. This disruption greatly increased the anti-PCa efficacy of the AR antagonist bicalutamide. In conclusion, we present a novel anti-PCa candidate and combination drug strategies to combat CRPC by intervening in the AR-AKT-HKII signaling network.

INTRODUCTION

Prostate cancer (PCa) is the second most common cancer and the fifth leading cause of cancer-related mortality in men.[1] Approximately 10 million men are currently diagnosed with PCa. Annually, PCa causes over 400,000 deaths globally, and this number is expected to exceed 800,000 by 2040.[1,2] The androgen receptor (AR) signaling plays a crucial role in the initiation and progression of PCa.[3] Androgen deprivation therapy (ADT) is a primary treatment for patients with advanced disease.[4] Typically, localized PCa is treated with delayed intervention or active local therapy, with or without ADT. Nevertheless, the efficacy of ADT differs across patients, and most of them typically develop castration resistant prostate cancer (CRPC) after 2–3 years of castration therapy.[5,6] Several AR-targeting therapies, including abiraterone, enzalutamide, and apalutamide, have been successfully developed in recent years to aid CRPC treatment. Nevertheless, innovative approaches in managing CRPC remain urgently needed.

The mechanisms underlying CRPC are complex, involving both AR-dependent and AR-independent resistance pathways. Alternatively, low or absent AR accumulation or activity can also contribute to castration resistance.[7] Recent research suggests a strong correlation between CRPC and the reprogramming of glucose metabolism along with hexokinase II (HKII) activation.[8–10] Many cancer cells exhibit a consistent metabolic phenotype through the reprogramming of their metabolic pathways from mitochondrial oxidative phosphorylation (OXPHOS) to aerobic glycolysis.[11] Hexokinase (HK) is the first rate-limiting enzyme in the glycolysis pathway. The subtype HKII has been discovered to be overexpressed in PCa, indicating it might serve as a novel biomarker of the disease with potential clinical applications.[12] AKT plays a significant role in regulating HKII, as its activation encourages the binding of HKII to the outer mitochondrial membrane, promoting glycolysis and inhibiting OXPHOS in tumor cells,[13] and preventing mitochondrial pathway-mediated apoptosis.[14,15] Furthermore, according to previous reports, Akt phosphorylates HK-II at Thr473,[16] which enhances its protein stability through a chaperone-mediated autophagy-mediated protein degradation pathway.[17]

The AR complex with androgen translocates into the nucleus and binds with androgen-response elements in promoter regions, thus regulating the transcription and expression of target genes involving with the growth of PCa cells (11, 12). Previous data show that AR is also highly expressed by most androgen-independent PCa, and increased in response to ADT, enhancing activation by residual androgens.[18–20] Bicalutamide is a first-generation anti-androgen FDA-indicated for use in combination therapy with an luteinizing hormone-releasing hormone

[1]Jiangsu Key Laboratory of Carcinogenesis and Intervention, China Pharmaceutical University, 24 Tongjiaxiang, Nanjing 210009, the People's Republic of China
[2]Pharmaceutical Animal Experiment Center, China Pharmaceutical University, 24 Tongjiaxiang, Nanjing 210009, the People's Republic of China
[3]Nanjing University of Chinese Medicine, 138 Xianlin Rd, Nanjing 210023, the People's Republic of China
[4]Department of Oncology, Huai'an Second People's Hospital, The Affiliated Huai'an Hospital of Xuzhou Medical University, Huaian, the People's Republic of China
[5]These authors contributed equally
[6]Lead contact
*Correspondence: 435204445@qq.com (Y.G.), wlbiws_1986@aliyun.com (L.W.)
https://doi.org/10.1016/j.isci.2024.109246

This is an open access article under the CC BY-NC-ND license (http://creativecommons.org/licenses/by-nc-nd/4.0/).

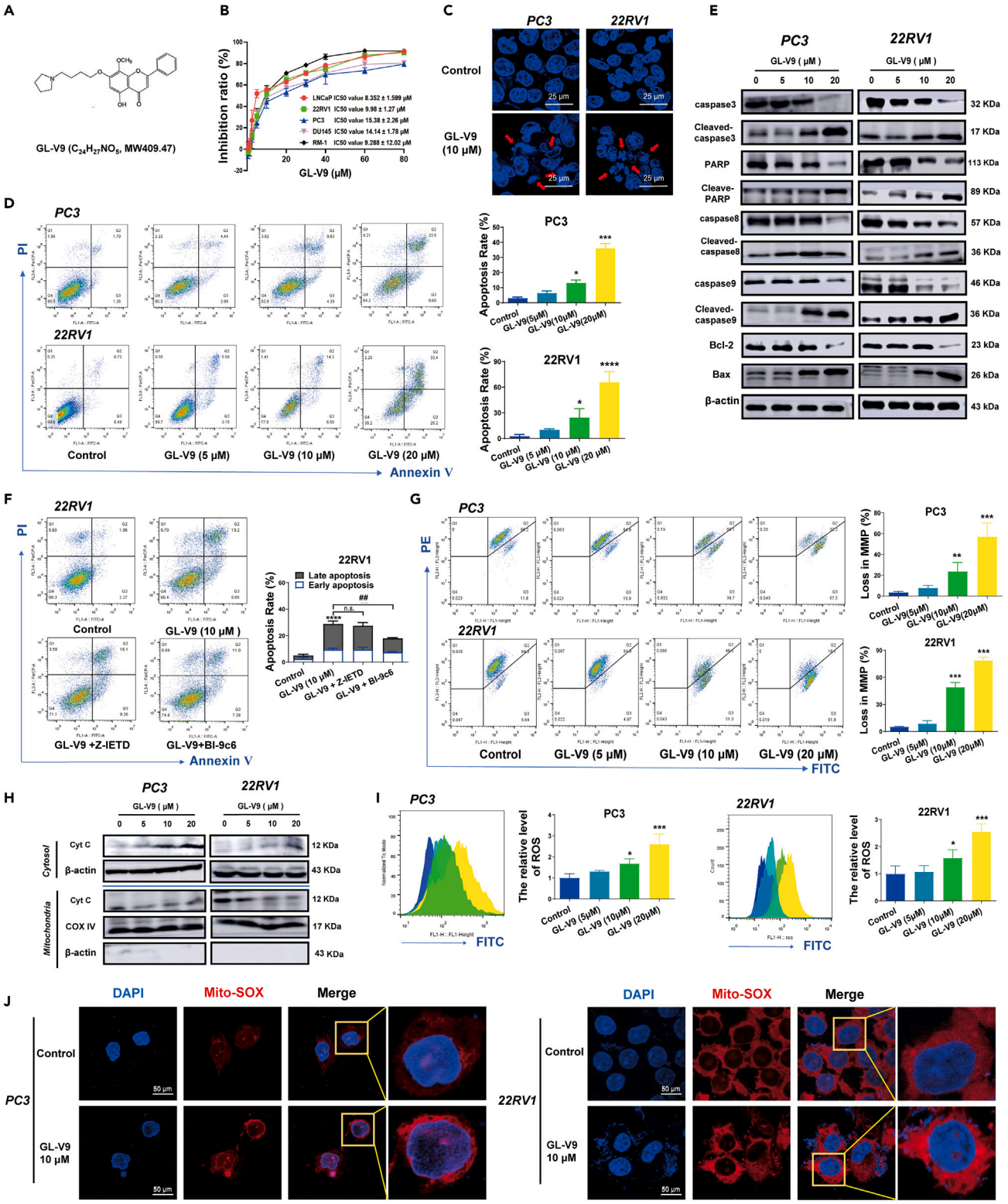

Figure 1. GL-V9 predominantly induces mitochondria-mediated apoptosis in PCa cells

(A) Chemical structure of GL-V9 ($C_{24}H_{27}NO_5$, MW409.47).

(B) CCK-8 kit assays for cell growth inhibition of 22RV1, LNCaP, DU145, PC3 and RM-1 cells treated with a series of concentrations of GL-V9 (0–100 μM) for 48 h.

(C) Morphological changes of cell nucleus in PC3 and 22RV1 cells treated with 10 μM GL-V9 were observed by DAPI staining. Scale bar, 25 μm.

CellPress
OPEN ACCESS

Figure 1. *Continued*

(D) Annexin-V/PI double-staining assay of 22RV1 and PC3 cells. Histograms of apoptosis rates were quantitated using both early and late apoptotic rates.
(E) Western blot assays for the expression of apoptosis-associated proteins in 22RV1 and PC3 cells.
(F) Annexin-V/PI double-staining assay of 22RV1 cells treated with GL-V9 (10 μM) for 48 h in the presence or absence of Z-IETD-FMK (10 μM) or BI-6C9 (20 μM).
(G) JC-1 assay of 22RV1 and PC3 cells. The percentages of the loss of MMP were quantified.
(H) Western blot assays for the protein level of Cyt-c in mitochondrial and cytoplasm.
(I) ROS Fluorometric assay. The levels of ROS were quantified.
(J) Mitochondrial ROS was measured using mito-SOX by immunofluorescence. Scale bar, 50 μm. All the WB assays were performed in triplicate and repeated three times with similar results. Quantitative data are presented as the mean ± SD (n = 3). *n.s.* means no significance, *$p < 0.05$, **$p < 0.01$, ***$p < 0.001$, ****$p < 0.0001$ compared with control. $^{\#\#}p < 0.01$ compared with 10 μM GL-V9 group.

agonists (LHRH analog) approved for the treatment of stage D2 metastatic carcinoma of the prostate.[21] It is indicated that activated AKT can phosphorylate AR, enhancing its nuclear translocation and binding to target genes.[22,23] Moreover, *p*-AKT levels are elevated in androgen-deprived tumors.[24–26] Recent studies demonstrate that glucose-6-phosphate isomerase (GPI), restored and increased by AR inhibition, maintains glucose metabolism and energy homeostasis by redirecting the glucose flux from the AR-dependent pentose phosphate pathway (PPP) to glycolysis pathway, thereby reducing the growth inhibitory effect of the AR antagonist enzalutamide.[27] Furthermore, research has demonstrated that ipatasertib, a highly specific AKT inhibitor, improves the survival rate of PCa patients when used in combination with abiraterone.[28–30] These findings suggest that the crosstalk between metabolic reprogramming and AR signaling may offer new insights to overcome the resistance to AR-targeted therapy.

GL-V9 is a synthesized flavonoid derived from wogonin that is one of the main active components of Scutellaria baicalensis (Figure 1A). GL-V9 has been shown to inhibit the growth of several tumor cells[31,32] and trigger mitochondria-mediated apoptosis.[33,34] Here, we investigated the anticancer activity and underlying mechanisms of GL-V9 against PCa. Our studies demonstrated that GL-V9 regulated glucose catabolism and induced mitochondria-mediated apoptosis of PCa cells, and significantly overcome resistance to AR inhibition by regulating AR-AKT-HKII network.

RESULT

GL-V9 predominantly induces mitochondria-mediated apoptosis of PCa cells

Firstly, we investigated the effect of GL-V9 on the growth inhibition of human PCa cell lines, including 22RV1, LNCaP, PC3, DU145, and mouse PCa cell lines RM-1. As shown in Figure 1B, GL-V9 significantly inhibited the proliferation of both human PCa cell lines and mouse PCa cells lines in a concentration-dependent manner. Previous studies have reported that GL-V9 induces apoptosis in breast cancer cells by affecting mitochondrial function.[33,35] Morphological changes of DAPI-stained nuclei were observed in PC3 and 22RV1 cells. After treatment of GL-V9, the cell nucleus exhibited marked nuclear fragmentation and crimple compared to untreated cells (Figure 1C). Moreover, apoptosis induction was further investigated in 22RV1 and PC3 cells through Annexin-V/PI double-staining assay. GL-V9 induced apoptosis of 22RV1 and PC3 cells in a concentration-dependent manner (Figure 1D). Western blot assay indicated that GL-V9 increased the cleavage of caspase 3, caspase 8, caspase 9, and PARP in 22RV1 and PC3 cells (Figure 1E). Additionally, GL-V9 resulted in upregulation of BAX and downregulation of BCL-2, which are both crucial constituents of the mitochondrial pathway-mediated apoptosis.[36] These findings suggest that GL-V9 may interfere with both the death receptor pathway and the mitochondrial pathway of apoptosis in PCa cells. A specific inhibitor of BH3 interacting domain (Bid), BI-6c9, can prevent cells from experiencing mitochondrial apoptosis and caspase-independent cell death in neurons.[37] Results demonstrated that apoptosis triggered by GL-V9 was significantly suppressed by BI-6c9 (Figure 1F). However, a selective caspase 8 inhibitor, Z-IETD-FMK (Z-IE(OMe)TD(OMe)-FMK),[38] could not influence the effect of GL-V9. Furthermore, GL-V9 caused concentration-dependent loss of mitochondrial membrane potential (MMP) (Figure 1G), release of Cyt-c from mitochondrial (Figure 1H), and increase in total reactive oxygen species (ROS) as well as mitochondrial ROS (Figures 1I and 1J). Taken together, these findings suggest that GL-V9 induces apoptosis of PCa cells via the mitochondrial pathway, rather than the death receptor pathway.

GL-V9 decreases expression of key enzymes involved in the glycolytic pathway and restricts glucose catabolism of PCa cells

Numerous studies suggest that cancer cells increase glycolysis to evade apoptosis induced by chemotherapy drugs.[39] Cancer cells commonly exhibit aerobic glycolysis and circumvent mitochondrial OXPHOS. This enables cancer cells to outcompete with normal cells for glucose uptake while evading the harmful effect of excessive ROS accumulation.[40] Our findings indicate that GL-V9 mainly induces apoptosis via the mitochondrial pathway, and we hypothesize that GL-V9 impacts glycolysis. Remarkably, when PC3 and 22RV1 cells were treated with GL-V9 for 24 h, there was a decrease in glucose uptake, lactate production, and ATP generation (Figures 2A–2C). Thus, GL-V9 potentially decreases the glycolytic capacity of PCa cells. In subsequent studies, we assessed the extracellular acidification rate (ECAR) and oxygen consumption rate (OCR) of 22RV1 and PC3 cells using the Seahorse glycolysis stress test and mitochondrial stress test. The results demonstrate that GL-V9 significantly reduced both ECAR and OCR (Figures 2D and 2E), which are crucial indicators of glycolysis and mitochondrial respiration, respectively. Therefore, GL-V9 curbs the glycolytic pathway and restricts glucose catabolism to produce ATP in PCa cells. Subsequently, the expression of enzymes involved in the glycolytic pathway was assessed. As shown in Figure 2F, GL-V9 notably decreased protein level of HKII, phosphofructokinase (PFKM), pyruvate kinases M1 (PKM1), and lactate dehydrogenase A (LDH-A) in 22RV1 and PC3 cells. PKM2 expression remained unchanged. We found that the addition of exogenous pyruvate sodium and the pyruvate kinase activator TEPP-46

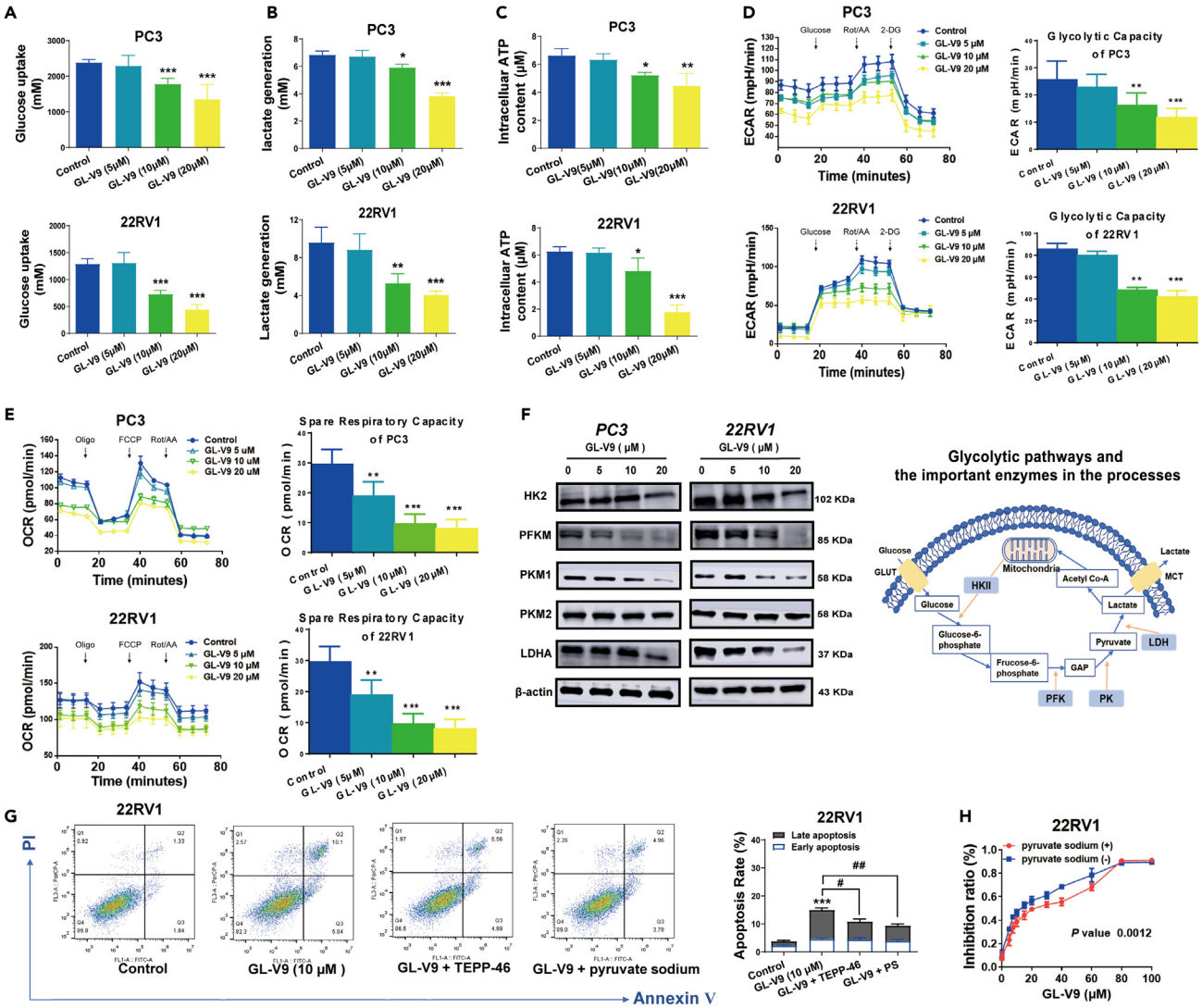

Figure 2. GL-V9 inhibits the glycolytic pathway and restricts the glucose catabolism of PCa cells

(A–F) Cells were treated with GL-V9 for 24 h. (A) Glucose uptake was measured with Amplex Red Glucose/Glucose Oxidase Assay Kit. (B) Lactate generation was measured with Lactic Acid Detection kit. (C) ATP production was measured with ATP assay kit. (D) Representative ECAR analysis was measured by Seahorse XF96e Analyzer and their responses to glucose, Rot/AA, and 2-deoxyglucose (2-DG) (n = 5 technical replicates). (E) Representative OCR analysis was measured by Seahorse XF96e Analyzer and their responses to oligomycin (oligo), FCCP, and rotenone plus antimycin A (Rot/AA) (n = 5 technical replicates). (F) The protein expressions of enzymes related to the glycolytic pathway were analyzed using western blotting (WB).

(G) Annexin-V/PI double-staining assay was performed on 22RV1 cells treated with a combination of GL-V9 with or without 10 mM pyruvate sodium (PS) or 40 μM TEPP-46 for 48 h.

(H) CCK-8 kit assays for cell growth of 22RV1 cells treated with 10 μM GL-V9 with/without 10 mM pyruvate sodium for 48 h. Quantitative data are presented as the mean ± SD (n = 3). *$p < 0.05$, **$p < 0.01$, ***$p < 0.001$, ****$p < 0.0001$ compared with control. $^{\#}p < 0.05$, $^{\#\#}p < 0.01$ compared with 10 μM GL-V9 group.

prevented GL-V9-induced cell apoptosis and growth inhibition (Figures 2G and 2H). This finding suggests that the glycolytic pathway plays a significant role in the anti-prostate cancer effects of GL-V9. Therefore, GL-V9 regulates the glycolytic pathway and restricts glucose catabolism of PCa cells.

GL-V9 inhibits the mitochondrial translocation of HKII and induces apoptosis in PCa cells by inactivating the AKT-HKII signaling pathway

Previous research has demonstrated that HKII functions as the rate-limiting enzyme in the glycolytic pathway and inhibits mitochondria pathway-mediated apoptosis by binding to the outer mitochondrial membrane.[41,42] GL-V9 lowered the total protein level of HKII. Hence, we investigated the impact of GL-V9 on mitochondrial HKII in human PCa. GL-V9. Our findings showed that GL-V9 consistently reduced

CellPress
OPEN ACCESS

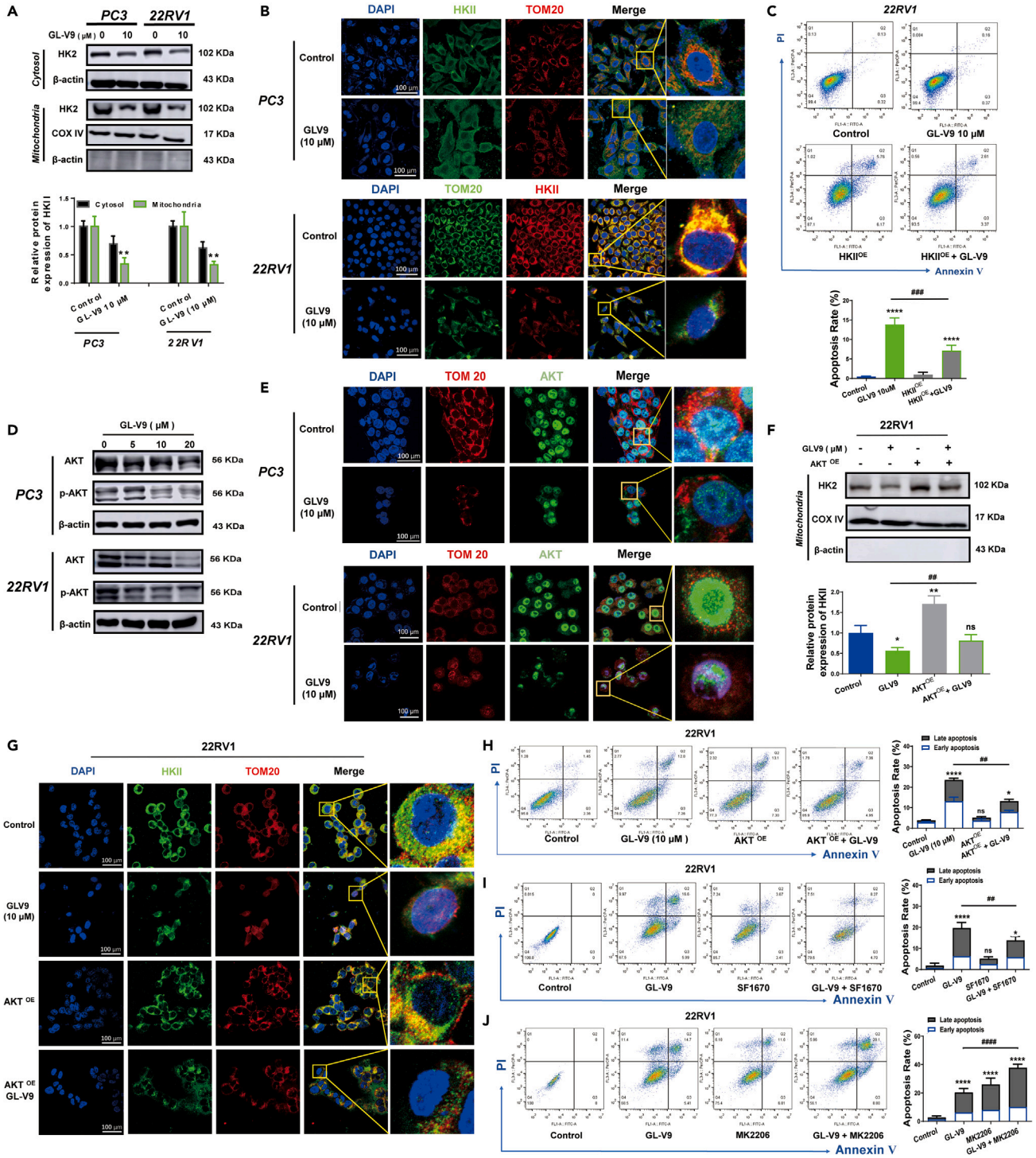

Figure 3. GL-V9 inhibits the mitochondrial translocation of HKII and induces apoptosis in PCa cells by inactivating the AKT-HKII signaling pathway

(A) Cells were treated with GL-V9 for 48 h. Western blot assays for the expression of HKII in mitochondria and cytoplasm of PC3 and 22RV1 cells.

(B) Mitochondrial localization of HKII in PC3 and 22RV1 cells treated with 10 μM GL-V9 was measured by immunofluorescence. Scale bar, 100 μm.

(C) Annexin-V/PI double-staining assay of HKII-overexpressed 22RV1 ($HKII^{OE}$ 22RV1) cells treated with/without 10 μM GL-V9.

(D) Protein expression of AKT and *p*-AKT.

(E) Mitochondrial localization of AKT in PC3 and 22RV1 cells treated with 10 μM GL-V9 was measured by immunofluorescence. Scale bar, 100 μm.

(F) The level of HKII protein in mitochondria of AKT^{OE} 22RV1 cells was analyzed after the treatment of 10 μM GL-V9 for 48 h.

Figure 3. *Continued*

(G) The mitochondria localization of HKII of AKT^{OE} 22RV1 cells. Scale bar, 100 μm.

(H) Annexin-V/PI double-staining assay of AKT-overexpressed 22RV1 (AKT^{OE} 22RV1) cells treated with/without 10 μM GL-V9 for 48 h.

(I and J) The apoptosis rate of 22RV1 cells treated with 10 μM GL-V9, in the present of/without 1 μM SF1670 or 10 μM MK2206 for 24 h, was analyzed. Quantitative data are presented as the mean ± SD (n = 3). *p < 0.05, **p < 0.01, ***p < 0.001, ****p < 0.0001 compared with control. #p < 0.05, ##p < 0.01, ####p < 0.0001 compared with 10 μM GL-V9 group.

the protein level of HKII in both mitochondria and cytoplasm of 22RV1 and PC3 cells (Figure 3A). The results of the immunofluorescence analysis indicted that GL-V9 decreased the mitochondrial localization of HKII in PCa cells (Figure 3B). When HKII was overexpressed in 22RV1 cells, the ability of GL-V9 to induce apoptosis was diminished, indicating that HKII plays a crucial role in the anti-PCa effect of GL-V9 (Figure 3C). Previous reports have suggested that Akt phosphorylates HK-II at Thr-473, thereby increasing the binding of HKII to mitochondria.[16] As demonstrated in Figures 3D and 3E, the protein expression of AKT and *p*-AKT, as well as the mitochondrial location of AKT, were significantly reduced by GL-V9. Moreover, the reduction in mitochondrial HKII triggered by GL-V9 was restored by overexpression of AKT in 22RV1 cells (Figures 3F and 3G). Overexpressing AKT reduced the GL-V9-induced apoptosis as well (Figure 3H). Additionally, the AKT activator SF1670, which activates AKT by suppressing PTEN,[43] partially obstructed GL-V9-induced apoptosis of 22RV1 (Figure 3I). Conversely, the highly selective allosteric Akt inhibitor MK2206 promoted the GL-V9-induced apoptosis of PCa cells (Figures 3J and S1A). Based on these results, it can be concluded that GL-V9 induces apoptosis of PCa cells by preventing the mitochondrial localization of HKII and inactivating AKT-HKII signaling.

GL-V9 improves anti-PCa activity of AR inhibitor by hindering the feedback activation of the AKT-controlled glycolytic pathway and mitochondrial localization of HKII

AR regulates the transcription of genes related to growth factors, inflammatory cytokines, and other functions.[44] Our findings indicate GL-V9 induces significant apoptosis in both AR-expressing 22RV1 cells and AR-negative PC3 cells. Further investigations were carried out to determine the effect of GL-V9 on AR signals in 22RV1 cells. As shown Figures 4A and 4B, GL-V9 downregulated the protein and mRNA levels of AR in 22RV1 cells, in addition to decreasing the level of activated p-AR. Furthermore, GL-V9 notably inhibited the nuclear localization of p-AR (Ser81) in 22RV1 (Figure 4C). Thus, GL-V9 suppressed the expression and activity of AR.

Targeting the AR pathway remains a primary strategy in treating metastatic PCa, given the critical role of AR signaling in driving the disease. Although second-generation AR antagonists offer a temporary response, resistance eventually develops.[45] Our study demonstrates that bicalutamide, a classical AR inhibitor, effectively inhibited the growth of 22RV1 cells (Figure 4D). Treatment of 50 μM bicalutamide for 24 h showed negligible effect on inducing apoptosis in 22RV1 cells. However, combination of GL-V9 (10 μM) with bicalutamide showed synergistic effects in cell growth inhibition (Figures 4D and 4E). GL-V9 (10 μM) co-treatment with bicalutamide resulted in a significant enhancement in apoptosis rate (Figure 4F). Prior investigations have suggested that AR inhibition can advance glucose metabolism. Hence, we examined the impacts of bicalutamide on enzymes and proteins related to the glycolytic pathway. The expression of AKT, *p*-AKT, and key enzymes in glycolytic pathway, including HKII, PFKM, LDHA, were significantly upregulated after 48 h bicalutamide treatment (Figures 4G and 4H). Additionally, bicalutamide promoted the mitochondrial localization of HKII in 22RV1 cells. The previous effects of 75 μM bicalutamide were reversed by 10 μM GL-V9 (Figures 4I and 4J).

To further investigate the influence of AKT in the bicalutamide-induced effect, we conducted a study combining the AKT inhibitor MK2206 with bicalutamide. The results showed that combination 10 μM MK2206 with bicalutamide effectively reduced the elevated levels of HKII, AKT, *p*-AKT, and LDHA protein, along with a change in the mitochondrial localization of HKII in 22RV1 cells (Figures S1B–S1D). Additionally, the combination of 10μM MK2206 with 75μM bicalutamide significantly increased apoptosis (Figure S1E). Overall, these findings suggest that GL-V9 improves the anti-PCa effect of bicalutamide by inhibiting the AKT-mediated glycolytic pathway and the mitochondrial localization of HKII. This pathway may potentially be reactivated by the AR inhibitor.

GL-V9 regulates AR-AKT-HKII signaling and inhibits the growth of human prostate tumor xenograft

Finally, we investigated the *in vivo* anti-PCa effects of GL-V9 using xenograft models of the 22RV1 or PC3 cells in nude mice. The results, shown in Figures 5A–5C, indicate that impede 150 mg/kg GL-V9 significantly impeded tumor growth and exhibited the same inhibitory effect as 30 mg/kg 5-fluorouracil (5-Fu) administered intravenously. Furthermore, oral administration of 300 mg/kg GL-V9 orally inhibited tumor growth much more efficiently than 5-Fu. To assess the potential toxicity of GL-V9 *in vivo*, we monitored the weight of mice and conducted blood routine and biochemical function tests. Additionally, we examined the heart, liver, spleen, lungs, and kidneys for any damage using hematoxylin and eosin (H&E) staining after the administration. As shown in Figures 5D–5F and Table S1, both 150 mg/kg and 300 mg/kg GL-V9 did not cause any toxicity or harm to the mice. However, the 5-Fu significantly reduced the weight of mice. Further investigations revealed that GL-V9 downregulated the expression of AKT, HKII, and AR in tumor tissue, while upregulating cleaved-caspase3 through an immunohistochemistry (IHC) assay (Figure 6A). Additionally, an immunofluorescence assay of tumor tissue revealed that GL-V9 reduced the nuclear localization of AR and the co-localization of HKII in mitochondria through an immunofluorescence assay of tumor tissue (Figures 6B–6D). These effects were not observed in the 5-Fu treatment group.

GL-V9 enhanced the efficacy of clinical drug bicalutamide for the treatment of PCa

5-FU is a broad-spectrum antitumor drug that functions that inhibits thymidine nucleotide synthase, effectively treating gastrointestinal cancer and other solid tumors. However, due to its commonly occurring toxic side effects, it is not used to treat tumors when better treatment options

CellPress
OPEN ACCESS

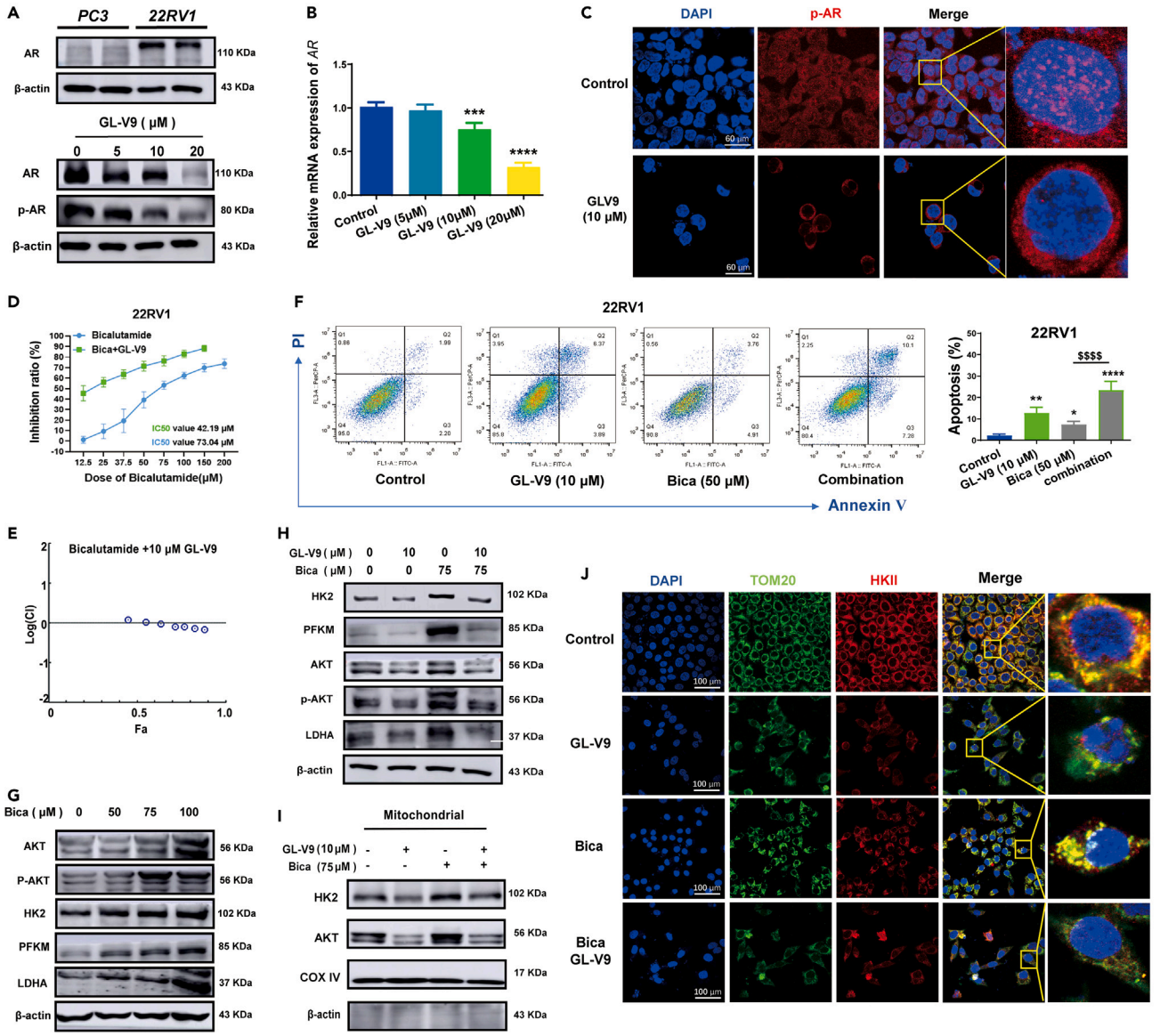

Figure 4. GL-V9 enhances anti-PCa activity of bicalutamide by hindering the feedback activation of the AKT-regulated glycolytic pathway and mitochondrial localization of HKII

(A) The protein expressions of AR and p-AR. 22RV1 cells were treated with GL-V9 for 48 h.

(B) The mRNA expressions of *AR*.

(C) The nuclear localization of p-AR in 22RV1. Scale bar, 60 μm.

(D) Cell growth inhibition of 22RV1 cells treated with bicalutamide or the combination of GL-V9 (10 μM) with bicalutamide for 24 h by CCK-8 assay.

(E) The combination index values for the combination of 1 bicalutamide (12.5, 25, 37.5, 50, 75, 100 or 150 μM, respectively) with 10 μM GL-V9 in22RV1 cells. The Fa values range from 0 to 1. CI < 1, synergism; CI = 1, additive effect and CI > 1, antagonism.

(F) Apoptosis of 22RV1 cells were treated with 10 μM GL-V9 with or without 25 μM bicalutamide for 24 h.

(G and H) The protein expression of HKII, PFKM, AKT, *p*-AKT and LDHA in 22RV1. (G) Cells were treated with bicalutamide for 24 h. (H) Cells were treated with 10 μM GL-V9 with or without 75 μM Bicalutamide.

(I) The protein level of mitochondrial HKII and AKT.

(J) The mitochondrial localization of HKII in 22RV1 cells treated with 10 μM GL-V9 with/without 75 μM bicalutamide. Scale bar, 100 μm. Quantitative data are presented as the mean ± SD (n = 3). *p < 0.05, **p < 0.01, ***p < 0.001, ****p < 0.0001 compared with 10 μM GL-V9 group. $$$$p < 0.0001 compared with bicalutamide group.

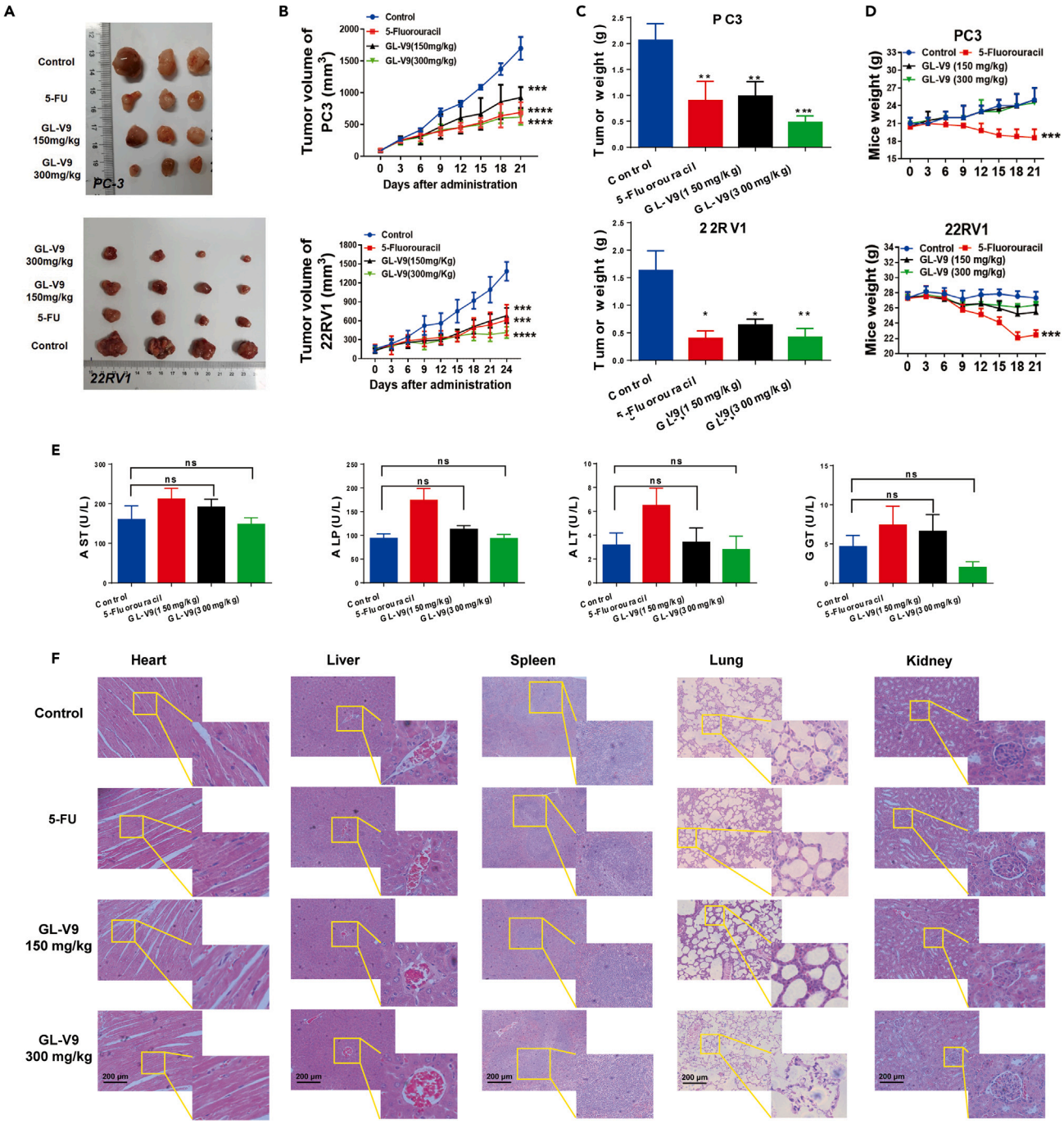

Figure 5. GL-V9 inhibits the growth of human prostate tumor xenograft with little toxicity

22RV1 and PC3 cells xenografted mouse models was established. Mice were administrated with GL-V9 (150/300 mg/kg, p.o., once daily), 5-fluorouracil (30 mg/kg, i.v., every three days), and sacrificed on day 24 after drugs administration.

(A–D) Photos for transplanted tumor, tumor volume, tumor weight and nude mice weight were shown, respectively.

(E) The serum levels of AST, ALP, GGT, and ALT in PC3 cells xenografted mice.

(F) H&E staining of organs in 22RV1 cells xenografted mice. Scale bar, 200 μm. Quantitative data are presented as the mean ± SD (n = 8). *ns* means no significance, *p < 0.05, **p < 0.01, ***p < 0.001, ****p < 0.0001 compared with control group.

CellPress
OPEN ACCESS

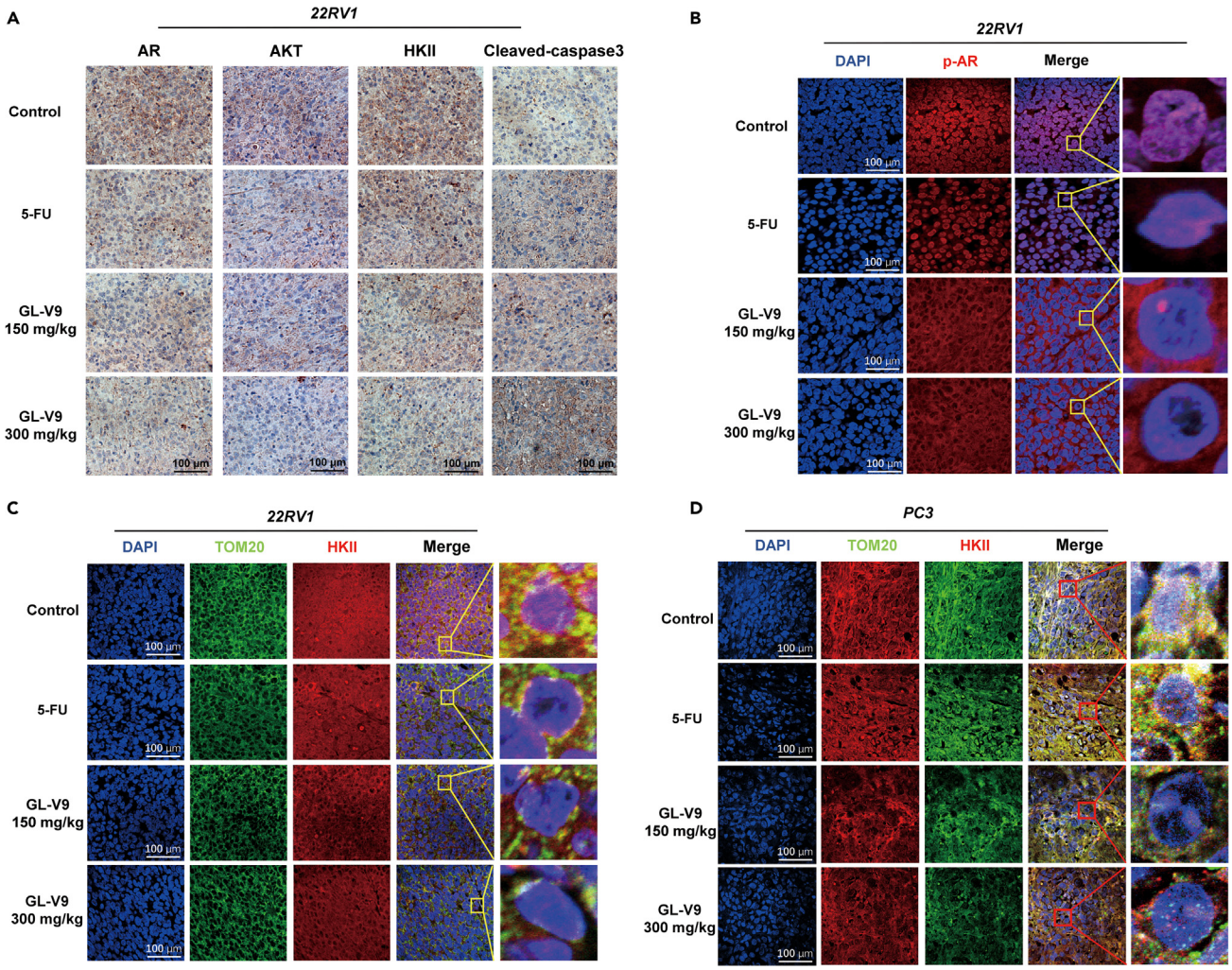

Figure 6. GL-V9 regulates the AR-AKT-HKII signaling of tumor tissue from the xenograft models

(A) IHC assay for the expressions of HKII, AKT, AR and Cleaved-caspase 3 in tumor tissues. Scale bar, 100 μm.

(B) Nuclear localization of AR in tumor tissues by immunofluorescence staining. Scale bar, 100 μm.

(C and D) The localization of HKII in mitochondria of tumor tissues of 22RV1 or PC3 cells xenografted mice. Scale bar, 100 μm.

are available in clinical practice. To assess the clinical research value of GL-V9, we re-evaluated its anti-PCa effect *in vivo* using the positive drugs bicalutamide and docetaxel, which are currently first-line clinical drugs. Docetaxel (Taxotere)-based regimens can be included among the most effective treatment options for the management of patients with advanced, androgen-independent PCa.[46] As shown in Figures 7A–7D, in AR-negative PCa cell lines PC3 xenograft model, GL-V9 (300 mg/kg, p.o.) demonstrated comparable tumor suppression to docetaxel (10 mg/kg, p.o.). In AR-expressing PCa cell lines 22RV1 xenograft model, GL-V9 not only exhibited better tumor growth inhibition than bicalutamide, but also enhanced its anti-PCa effect (Figures 7E–7H). In addition to conventional evaluation methods for anticancer effects in xenograft models, we also used tumor growth delay as the evaluating indicator to determine anti-PCa activity. Tumor growth delay activity provides stronger evidence of clinical potential than tumor growth inhibition activity.[47] Xenograft models were created using 22RV1 cells and treated with GL-V9 (300 mg/kg, p.o) and bicalutamide (20 mg/kg, p.o) either alone or in combination for 12 days. Administration was then withdrawn and the models were sacrificed on day 27. The results indicate that the combination of GL-V9 and bicalutamide resulted in a stronger delay in tumor growth compared to either treatment alone (Figures 7I–7L).

DISCUSSION

Hormone drugs that target AR play a pivotal role in treating PCa and are frequently used from early local disease to later distant metastatic disease.[48,49] ADT is the most common form of hormone therapy used in clinics, even though almost all patients who receive this therapy have developed CRPC and eventually metastatic castration-resistant prostate cancer (mCRPC).[50,51] New drugs that inhibit AR signal have been developed because AR remains active in mCRPC. Abiraterone (Zytiga, Johnson) and Enzalutamide (Xtandi, Pfizer) are the first AR-targeted therapies

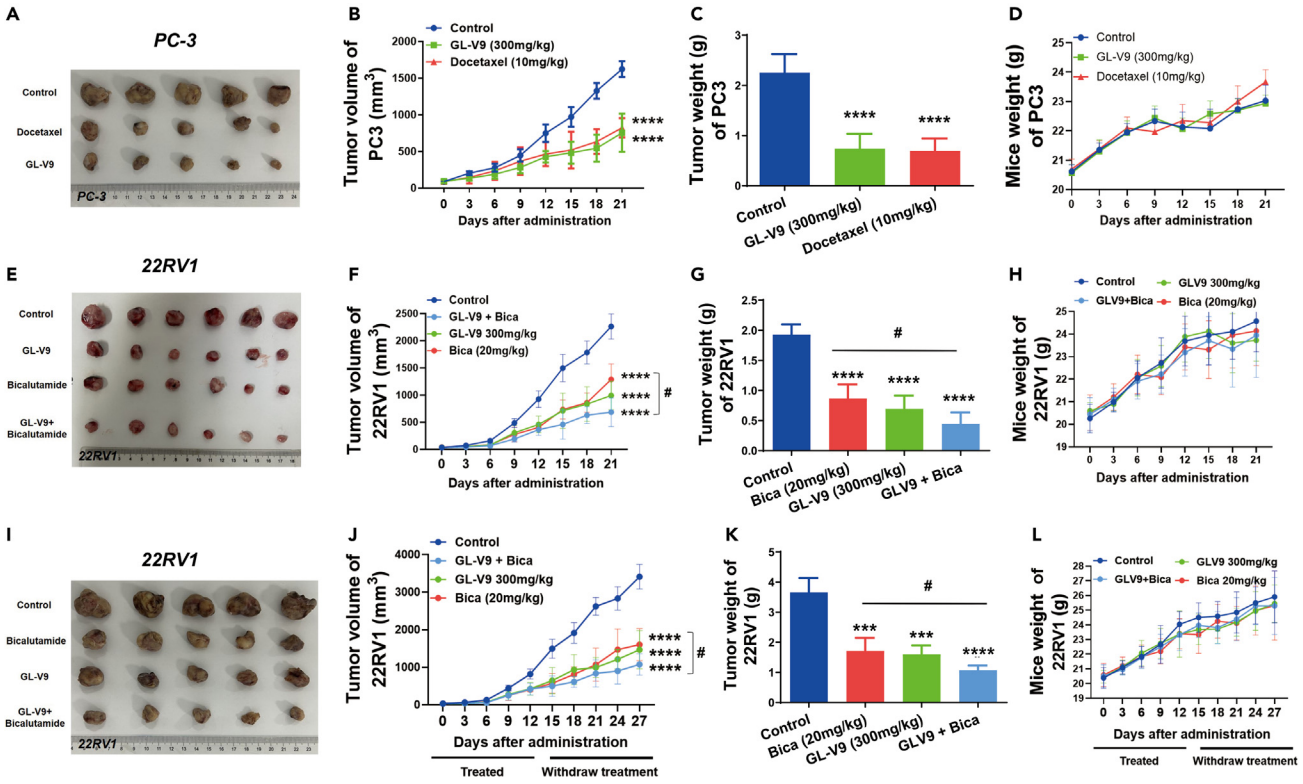

Figure 7. GL-V9 enhanced the efficacy of clinical drug bicalutamide for the treatment of PCa

(A–D) PC3 cell xenograft model mice were treated with GL-V9 (300 mg/kg, p.o., once daily), docetaxel (10 mg/kg, p.o., once daily) or a combination of both. Photos for transplanted tumor, tumor volume, tumor weight and nude mice weight were shown, respectively.

(E–H) 22RV1 cell xenograft model mice were treated with GL-V9 (300 mg/kg, p.o., once daily), bicalutamide (20 mg/kg, p.o, once daily) or a combination of both. Photos for transplanted tumor, tumor volume, tumor weight and nude mice weight were shown, respectively.

(I–L) 22RV1 cell xenograft model mice were GL-V9 (300 mg/kg, p.o) and bicalutamide (20 mg/kg, p.o) either alone or in combination for 12 days. Administration was then withdrawn and the models were sacrificed on day 27. Photos for transplanted tumor, tumor volume, tumor weight and nude mice weight were shown, respectively. Quantitative data are presented as the mean ± SD (n = 6). *ns* means no significance, *$p < 0.05$, **$p < 0.01$, ***$p < 0.001$, ****$p < 0.0001$ compared with control group. $^{\#}p < 0.05$ compared between bicalutamide alone group and the combination group.

approved for the treatment of mCRPC, and are considered the first-line standard treatment.[52–54] Moreover, there are emerging therapies for mCPRC, such as PARP inhibitors (Olaparib, Rucaparib),[55] Prostate-specific membrane antigen (PSMA) targeted radiopharmaceutical therapy (Lu-PSMA-617, TLX591),[56] AKT inhibitors (ipatasertib, capivasertib),[57] and PD1 inhibitors (pembrolizumab, nivolumab),[58] which are at various stages of development and testing. Additionally, GL-V9, a synthesized flavonoid derived from the natural product wogonin, has been confirmed to be an effective antineoplastic drug.[59] Our study shows that GL-V9 has potent anticancer activity in both AR-negative and AR-expressing PCa by intervening in the interactive of AR-AKT-HKII signaling networks (Figure 8). In AR-negative PCa cells, GL-V9 destabilizes HKII protein and preventsits localization in the mitochondria by deactivating AKT and inhibiting HK-II phosphorylation at Thr473. This leads to cell growth inhibition and mitochondrial pathway-mediated apoptosis. Whereas in AR-expressing PCa cells, AKT-regulated glycolytic pathway and the mitochondrial localization of HKII can potentially be feedback activated by the AR inhibitor, such as bicalutamide. GL-V9 not only regulates HKII-regulated glucose catabolism and apoptosis but also inhibits the expression, phosphorylation, and nuclear translocation of AR protein, thereby preventing feedback activation. This demonstrates a synergistic effect in anti-PCa effects with AR inhibitors, such as bicalutamide.

The PI3K/AKT pathway is associated with therapeutic resistance to anti-androgen therapy.[60,61] This is the fact that inhibition of AR leads to an increase in the activation of AKT pathway.[62] AKT inhibitors, such as ipatasertib, have been developed for the treatment of mCRPC. Encouraging outcomes were achieved in the study of combined treatment with Abiterone for mCRPC.[28,63] PTEN is one of the most important tumor suppressors. Recent research reveals that PTEN suppresses tumorigenesis by directly dephosphorylating Akt.[64] Genomic aberrations of the PTEN tumor suppressor gene are among the most common in PCa. Inactivation of PTEN by deletion or mutation is identified in ~20% of primary prostate tumor samples at radical prostatectomy and in as many as 50% of castration-resistant tumors.[65] Loss of PTEN function leads to activation of the PI3K-AKT pathway and is strongly associated with adverse oncological outcomes. It is reported that 22RV1 cells are PTEN-positive PCa cells,[66] and PC3 cells are PTEN-null.[67] Our results indicate that the inhibition of GL-V9 in PCa is not affected by PTEN status, showing potent anti-PCa effects in both 22RV1 cells and PC3 cells. Previous studies have shown that GL-V9 increases PTEN expression and induces degradation of AKT blocked PI3K/AKT signaling in T cell malignancies.[68] Additionally, GL-V9 promotes the subcellular localization of PTEN, resulting in an increase of

CellPress
OPEN ACCESS

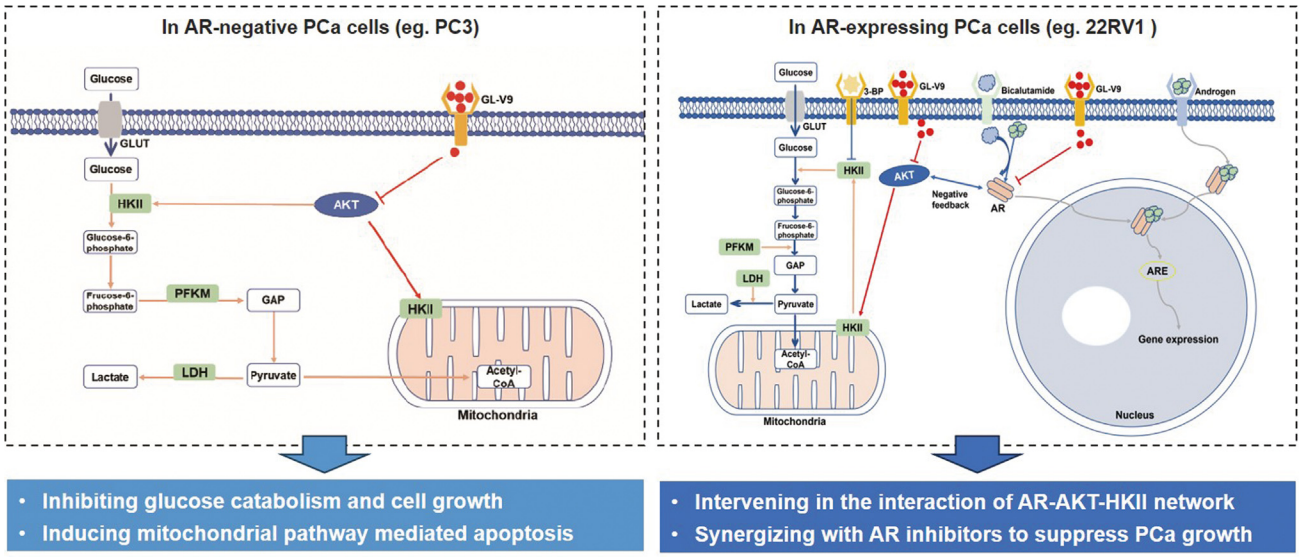

Figure 8. Schematic representation that GL-V9 inhibits prostate cancer by intervening in the interactive signaling networks of AR-AKT-HKII

The synthesized flavonoid GL-V9 is potent anti-PCa candidate and suppresses the growth in both AR-negative and AR-expressing PCa. In AR-negative PCa cells, GL-V9 downregulates the protein level and mitochondrial location of HKII by inactivating AKT induced-phosphorylation of HK-II, leading to cell growth inhibition and mitochondrial pathway mediated apoptosis. Whereas in AR-expressing PCa cells, AKT-regulated glycolytic pathway and the mitochondrial localization of HKII can potentially be feedback activated by the AR inhibitor. In addition to regulate HKII-regulated glucose catabolism and apoptosis, GL-V9 inhibits the expression, phosphorylation, and nuclear translocation of AR protein. This demonstrates a synergistic effect in anti-PCa effects with AR inhibitors, such as bicalutamide.

calcium release from endoplasmic reticulum (ER) and calcium-mediated mitochondrial dysfunction.[34] These results indicate that GL-V9 not only restores PTEN function but also interrupts AKT signal directly.

Additionally, AKT activation can enhance the expression of glucose transporter 1 (GLUT1) and its plasma membrane localization, and increase the activity of glycolysis enzyme HKII, thereby facilitating the capture of glucose entering cells through glycolysis and other pathways. Glycolysis intervention is of growing interest for treating mCRPC due to its potential to prevent the occurrence, progression, and chemotherapy resistance of PCa.[69] Prof. Liu and his colleagues discovered that targeted drugs, such as Skp2 inhibitors, can shift tumor cell metabolism from glycolysis to tricarboxylic acid cycle (TCA) cycle, inducing tumor cell growth inhibition in PCa cells.[70] Chelakkot et al. confirmed that the interaction between glucose metabolism and AR signals in breast and PCa, suggesting that combining endocrine therapy with metabolic regulators could become the standard treatment to overcome drug resistance.[71] AKT is involved in the transferring HKII from cytoplasm to mitochondria to initiate glycolysis. In Figures S2A–S2D, our study found that GL-V9 had superior inhibitory effects on cell growth and glycolytic capacity compared to 3-bromopyruvate (3-BP), a potent HKII inhibitor.[72,73] The inhibitory effects of 3-BP are diminished by the increased expression of AKT, and the combination of GL-V9 and 3-BP resulted in much stronger apoptosis of PCa cells than either treatment alone (Figures S2E–S2F).

In PCa, AKT is also a critical protein that phosphorylates and promotes the nuclear translocation of AR.[74] Bicalutamide, the most widely used AR antagonist, can promote stronger AKT-HKII signaling in AR-expressing 22RV1 cells. In addition to inhibiting AKT-HKII signaling, GL-V9 significantly suppresses the expression and activity of AR. The combination treatment of bicalutamide and GL-V9 effectively enhances anti-prostate cancer abilities. It is reported that bicalutamide does not function as an AR antagonist by preventing AR binding to DNA but instead stimulates the assembly of a transcriptionally inactive AR on DNA.[75] The findings indicate that the increased expression of AR and transcriptional coactivator proteins in androgen-independent PCa may decrease the efficacy of bicalutamide in blocking AR activation by residual androgens. Moreover, this mechanism predicts that inhibition of AR production in conjunction with bicalutamide (or potent AR antagonists) may have efficacy in androgen-independent PCa. Therefore, although GL-V9 decreased AR expression, the combined use of GL-V9 and bicalutamide is expected to show better efficacy in treating PCa.

All aforementioned, our study suggests that GL-V9 has unique advantages in combating PCa by regulating the interactive signaling networks of AR-AKT-HKII. This mechanism breaks through the inefficiency of AR inhibitors caused by the activation of enhanced AKT feedback, and bypass the side effects of AKT inhibitors. We provide a new anti-PCa candidate and combinatorial drug strategies to overcome CRPC.

Limitations of the study

The article demonstrates that GL-V9 induces apoptosis of PCa cells by regulating the AR-AKT-HKII signaling network. However, the specific target of GL-V9 for treating PCa still requires exploration. It is currently unknown whether GL-V9 inhibits the activation of AKT and AR through direct binding inhibition or by interfering with upstream signaling. Further evaluation is also necessary to determine the tumor selectivity of GL-V9 and its impact on normal prostate cells.

STAR★METHODS

Detailed methods are provided in the online version of this paper and include the following:

- KEY RESOURCES TABLE
- RESOURCE AVAILABILITY
  - Lead contact
  - Material availability
  - Data and code availability
- EXPERIMENTAL MODEL AND STUDY PARTICIPANT DETAILS
  - Mouse models
- METHOD DETAILS
  - Cell culture
  - Cell viability and apoptosis assays
  - Measurement of intracellular Reactive Oxygen Species (ROS) levels
  - Measurement of mitochondrial membrane potential (MMP)
  - Measurement of lactic acid production, glucose uptake and ATP generation
  - Measurement of ECAR and OCR
  - Gene expression studies (QPCR)
  - Immunofluorescence
  - Western blot
  - Immunohistochemistry (IHC)
  - Ethics
- QUANTIFICATION AND STATISTICAL ANALYSIS

SUPPLEMENTAL INFORMATION

Supplemental information can be found online at https://doi.org/10.1016/j.isci.2024.109246.

ACKNOWLEDGMENTS

This work was supported by the National Natural Science Foundation of China, China (no.82373907, no.82204442), Social Development Project of Jiangsu Provincial Key Research and Development Program, China (BE2021782), and Qinglan Project of Jiangsu Province of China, China.

AUTHOR CONTRIBUTIONS

L.W., R.W., and Y.G. provided direction and guidance throughout the preparation of this manuscript. R.W., Q.M., and Y.G. designed the experiments and conducted the main experiments. R.W., Q.M., Y.Z. collected and analyzed data. X.Z. and D.W. provided key experimental materials. L.W. and R.W. wrote and edited the manuscript. R.W., L.W., and Y.G. reviewed and made significant revisions to the manuscript. L.W. and Y.G. provided funding support. All authors read and approved the final manuscript.

DECLARATION OF INTERESTS

The authors declare no conflicts of interest.

Received: August 15, 2023
Revised: December 14, 2023
Accepted: February 13, 2024
Published: February 16, 2024

REFERENCES

1. Sung, H., Ferlay, J., Siegel, R.L., Laversanne, M., Soerjomataram, I., Jemal, A., and Bray, F. (2021). Global Cancer Statistics 2020: GLOBOCAN Estimates of Incidence and Mortality Worldwide for 36 Cancers in 185 Countries. CA. Cancer J. Clin. *71*, 209–249.
2. Sandhu, S., Moore, C.M., Chiong, E., Beltran, H., Bristow, R.G., and Williams, S.G. (2021). Prostate cancer. Lancet *398*, 1075–1090.
3. Lonergan, P.E., and Tindall, D.J. (2011). Androgen receptor signaling in prostate cancer development and progression. J. Carcinog. *10*, 20.
4. Ku, S.Y., Gleave, M.E., and Beltran, H. (2019). Towards precision oncology in advanced prostate cancer. Nat. Rev. Urol. *16*, 645–654.
5. Pungsrinont, T., Kallenbach, J., and Baniahmad, A. (2021). Role of PI3K-AKT-mTOR Pathway as a Pro-Survival Signaling and Resistance-Mediating Mechanism to Therapy of Prostate Cancer. Int. J. Mol. Sci. *22*, 11088.
6. Moll, J.M., Hofland, J., Teubel, W.J., de Ridder, C.M.A., Taylor, A.E., Graeser, R., Arlt, W., Jenster, G.W., and van Weerden, W.M. (2022). Abiraterone switches castration-resistant prostate cancer dependency from adrenal androgens towards androgen receptor variants and glucocorticoid receptor signalling. Prostate *82*, 505–516.
7. Thomas-Jardin, S.E., Dahl, H., Nawas, A.F., Bautista, M., and Delk, N.A. (2020). NF-kappaB signaling promotes castration-resistant

prostate cancer initiation and progression. Pharmacol. Ther. *211*, 107538.
8. Wang, L., Wang, J., Xiong, H., Wu, F., Lan, T., Zhang, Y., Guo, X., Wang, H., Saleem, M., Jiang, C., et al. (2016). Co-targeting hexokinase 2-mediated Warburg effect and ULK1-dependent autophagy suppresses tumor growth of PTEN- and TP53-deficiency-driven castration-resistant prostate cancer. EBioMedicine *7*, 50–61.
9. GuhaThakurta, D., Sheikh, N.A., Fan, L.Q., Kandadi, H., Meagher, T.C., Hall, S.J., Kantoff, P.W., Higano, C.S., Small, E.J., Gardner, T.A., et al. (2015). Humoral Immune Response against Nontargeted Tumor Antigens after Treatment with Sipuleucel-T and Its Association with Improved Clinical Outcome. Clin. Cancer Res. *21*, 3619–3630.
10. Feng, T., Wang, J., Cheng, K., Lu, Q., Zhao, R., Wang, S., Zhang, Q., Ge, L., Pan, J., Song, G., and Wang, L. (2021). IL13Rα1 prevents a castration resistant phenotype of prostate cancer by targeting hexokinase 2 for ubiquitin-mediated degradation. Cancer Biol. Med. *19*, 1008–1028.
11. DeBerardinis, R.J., and Chandel, N.S. (2020). We need to talk about the Warburg effect. Nat. Metab. *2*, 127–129.
12. Sun, X., Huang, Q., Peng, F., Wang, J., Zhao, W., and Guo, G. (2021). Expression and Clinical Significance of HKII and HIF-1α in Grade Groups of Prostate Cancer. Front. Genet. *12*, 680928.
13. Lou, Q., Zhang, M., Zhang, K., Liu, X., Zhang, Z., Zhang, X., Yang, Y., and Gao, Y. (2022). Arsenic exposure elevated ROS promotes energy metabolic reprogramming with enhanced AKT-dependent HK2 expression. Sci. Total Environ. *836*, 155691.
14. Shangguan, X., He, J., Ma, Z., Zhang, W., Ji, Y., Shen, K., Yue, Z., Li, W., Xin, Z., Zheng, Q., et al. (2021). SUMOylation controls the binding of hexokinase 2 to mitochondria and protects against prostate cancer tumorigenesis. Nat. Commun. *12*, 1812.
15. Xue, Y.N., Yu, B.B., Li, J.L., Guo, R., Zhang, L.C., Sun, L.K., Liu, Y.N., and Li, Y. (2019). Zinc and p53 disrupt mitochondrial binding of HK2 by phosphorylating VDAC1. Exp. Cell Res. *374*, 249–258.
16. Roberts, D.J., Tan-Sah, V.P., Smith, J.M., and Miyamoto, S. (2013). Akt phosphorylates HK-II at Thr-473 and increases mitochondrial HK-II association to protect cardiomyocytes. J. Biol. Chem. *288*, 23798–23806.
17. Yang, T., Ren, C., Qiao, P., Han, X., Wang, L., Lv, S., Sun, Y., Liu, Z., Du, Y., and Yu, Z. (2018). PIM2-mediated phosphorylation of hexokinase 2 is critical for tumor growth and paclitaxel resistance in breast cancer. Oncogene *37*, 5997–6009.
18. Hobisch, A., Culig, Z., Radmayr, C., Bartsch, G., Klocker, H., and Hittmair, A. (1995). Distant metastases from prostatic carcinoma express androgen receptor protein. Cancer Res. *55*, 3068–3072.
19. van der Kwast, T.H., Schalken, J., Ruizeveld de Winter, J.A., van Vroonhoven, C.C., Mulder, E., Boersma, W., and Trapman, J. (1991). Androgen receptors in endocrine-therapy-resistant human prostate cancer. Int. J. Cancer *48*, 189–193.
20. Taplin, M.E., Bubley, G.J., Shuster, T.D., Frantz, M.E., Spooner, A.E., Ogata, G.K., Keer, H.N., and Balk, S.P. (1995). Mutation of the androgen-receptor gene in metastatic androgen-independent prostate cancer. N. Engl. J. Med. *332*, 1393–1398.
21. Beebe-Dimmer, J.L., Ruterbusch, J.J., Bylsma, L.C., Gillezeau, C., Fryzek, J., Schultz, N.M., Flanders, S.C., Barlev, A., Heath, E., and Quek, R.G.W. (2018). Patterns of Bicalutamide Use in Prostate Cancer Treatment: A U.S. Real-World Analysis Using the SEER-Medicare Database. Adv. Ther. *35*, 1438–1451.
22. Yan, G., Ru, Y., Yan, F., Xiong, X., Hu, W., Pan, T., Sun, J., Zhang, C., Wang, Q., and Li, X. (2019). MIIP inhibits the growth of prostate cancer via interaction with PP1α and negative modulation of AKT signaling. Cell Commun. Signal. *17*, 44.
23. Palazzolo, I., Burnett, B.G., Young, J.E., Brenne, P.L., La Spada, A.R., Fischbeck, K.H., Howell, B.W., and Pennuto, M. (2007). Akt blocks ligand binding and protects against expanded polyglutamine androgen receptor toxicity. Hum. Mol. Genet. *16*, 1593–1603.
24. Waseem, D., Khan, G.M., Haq, I.U., Rashid, U., and Syed, D.N. (2020). The triphenyltin carboxylate derivative triphenylstannyl 2-(benzylcarbamoyl)benzoate impedes prostate cancer progression via modulation of Akt/FOXO3a signaling. Toxicol. Appl. Pharmacol. *401*, 115091.
25. Dulinska-Litewka, J., McCubrey, J.A., and Laidler, P. (2013). Increased Akt signaling resulting from the loss of androgen responsiveness in prostate cancer. Curr. Med. Chem. *20*, 144–157.
26. Jiménez-Vacas, J.M., Herrero-Aguayo, V., Montero-Hidalgo, A.J., Gómez-Gómez, E., Fuentes-Fayos, A.C., León-González, A.J., Sáez-Martínez, P., Alors-Pérez, E., Pedraza-Arévalo, S., González-Serrano, T., et al. (2020). Dysregulation of the splicing machinery is directly associated to aggressiveness of prostate cancer. EBioMedicine *51*, 102547.
27. Geng, H., Xue, C., Mendonca, J., Sun, X.X., Liu, Q., Reardon, P.N., Chen, Y., Qian, K., Hua, V., Chen, A., et al. (2018). Interplay between hypoxia and androgen controls a metabolic switch conferring resistance to androgen/AR-targeted therapy. Nat. Commun. *9*, 4972.
28. Sweeney, C., Bracarda, S., Sternberg, C.N., Chi, K.N., Olmos, D., Sandhu, S., Massard, C., Matsubara, N., Alekseev, B., Parnis, F., et al. (2021). Ipatasertib plus abiraterone and prednisolone in metastatic castration-resistant prostate cancer (IPATential150): a multicentre, randomised, double-blind, phase 3 trial. Lancet *398*, 131–142.
29. Cocco, S., Leone, A., Roca, M.S., Lombardi, R., Piezzo, M., Caputo, R., Ciardiello, C., Costantini, S., Bruzzese, F., Sisalli, M.J., et al. (2022). Inhibition of autophagy by chloroquine prevents resistance to PI3K/AKT inhibitors and potentiates their antitumor effect in combination with paclitaxel in triple negative breast cancer models. J. Transl. Med. *20*, 290.
30. Lin, K.H., Rutter, J.C., Xie, A., Killarney, S.T., Vaganay, C., Benaksas, C., Ling, F., Sodaro, G., Meslin, P.A., Bassil, C.F., et al. (2022). P2RY2-AKT activation is a therapeutically actionable consequence of XPO1 inhibition in acute myeloid leukemia. Nat. Cancer *3*, 837–851.
31. Zhao, J., Bai, D., Qi, L., Cao, W., Du, J., Gu, C., Zhou, C., Gao, Y., Zhang, L., Zhao, Y., and Lu, N. (2023). The flavonoid GL-V9 alleviates liver fibrosis by triggering senescence by regulating the transcription factor GATA4 in activated hepatic stellate cells. Br. J. Pharmacol. *180*, 1072–1089.
32. Zhao, Y., Guo, Q., Zhao, K., Zhou, Y., Li, W., Pan, C., Qiang, L., Li, Z., and Lu, N. (2017). Small molecule GL-V9 protects against colitis-associated colorectal cancer by limiting NLRP3 inflammasome through autophagy. OncoImmunology *7*, e1375640.
33. Yang, D., Tian, X., Ye, Y., Liang, Y., Zhao, J., Wu, T., and Lu, N. (2021). Identification of GL-V9 as a novel senolytic agent against senescent breast cancer cells. Life Sci. *272*, 119196.
34. Zhao, K., Li, G., Yao, Y., Zhou, Y., Li, Z., Guo, Q., and Lu, N. (2017). Activation of phospholipase C-γ1 and translocation of phosphatidylinositol-3,4,5-trisphosphate 3-phosphatase contribute to GL-V9-induced apoptosis in human gastric cancer cells. Exp. Cell Res. *356*, 8–19.
35. Yang, L., He, Z., Yao, J., Tan, R., Zhu, Y., Li, Z., Guo, Q., and Wei, L. (2018). Regulation of AMPK-related glycolipid metabolism imbalances redox homeostasis and inhibits anchorage independent growth in human breast cancer cells. Redox Biol. *17*, 180–191.
36. Valentini, E., D'Aguanno, S., Di Martile, M., Montesano, C., Ferraresi, V., Patsilinakos, A., Sabatino, M., Antonini, L., Chiacchiarini, M., Valente, S., et al. (2022). Targeting the anti-apoptotic Bcl-2 family proteins: machine learning virtual screening and biological evaluation of new small molecules. Theranostics *12*, 2427–2444.
37. Neitemeier, S., Jelinek, A., Laino, V., Hoffmann, L., Eisenbach, I., Eying, R., Ganjam, G.K., Dolga, A.M., Oppermann, S., and Culmsee, C. (2017). BID links ferroptosis to mitochondrial cell death pathways. Redox Biol. *12*, 558–570.
38. Ke, D.Q., Chen, Z.Y., Li, Z.L., Huang, X., and Liang, H. (2020). Target inhibition of caspase-8 alleviates brain damage after subarachnoid hemorrhage. Neural Regen. Res. *15*, 1283–1289.
39. Li, F.L., Liu, J.P., Bao, R.X., Yan, G., Feng, X., Xu, Y.P., Sun, Y.P., Yan, W., Ling, Z.Q., Xiong, Y., et al. (2018). Acetylation accumulates PFKFB3 in cytoplasm to promote glycolysis and protects cells from cisplatin-induced apoptosis. Nat. Commun. *9*, 508.
40. Ganapathy-Kanniappan, S. (2018). Molecular intricacies of aerobic glycolysis in cancer: current insights into the classic metabolic phenotype. Crit. Rev. Biochem. Mol. Biol. *53*, 667–682.
41. Wu, R., Wyatt, E., Chawla, K., Tran, M., Ghanefar, M., Laakso, M., Epting, C.L., and Ardehali, H. (2012). Hexokinase II knockdown results in exaggerated cardiac hypertrophy via increased ROS production. EMBO Mol. Med. *4*, 633–646.
42. Woldetsadik, A.D., Vogel, M.C., Rabeh, W.M., and Magzoub, M. (2017). Hexokinase II-derived cell-penetrating peptide targets mitochondria and triggers apoptosis in cancer cells. FASEB J *31*, 2168–2184.
43. Wen, Z., Mai, Z., Zhu, X., Wu, T., Chen, Y., Geng, D., and Wang, J. (2020). Mesenchymal stem cell-derived exosomes ameliorate cardiomyocyte apoptosis in hypoxic conditions through microRNA144 by targeting the PTEN/AKT pathway. Stem Cell Res. Ther. *11*, 36.
44. Lu, X., Fong, K.W., Gritsina, G., Wang, F., Baca, S.C., Brea, L.T., Berchuck, J.E., Spisak, S., Ross, J., Morrissey, C., et al. (2022). HOXB13 suppresses de novo lipogenesis through HDAC3-mediated epigenetic reprogramming in prostate cancer. Nat. Genet. *54*, 670–683.

45. Chen, Y., Zhou, Q., Hankey, W., Fang, X., and Yuan, F. (2022). Second generation androgen receptor antagonists and challenges in prostate cancer treatment. Cell Death Dis. *13*, 632.
46. Logothetis, C.J. (2002). Docetaxel in the integrated management of prostate cancer. Current applications and future promise. Oncology (Williston Park) *16*, 63–72.
47. Teicher, B.A. (2006). Tumor models for efficacy determination. Mol. Cancer Ther. *5*, 2435–2443.
48. Crawford, E.D., Heidenreich, A., Lawrentschuk, N., Tombal, B., Pompeo, A.C.L., Mendoza-Valdes, A., Miller, K., Debruyne, F.M.J., and Klotz, L. (2019). Androgen-targeted therapy in men with prostate cancer: evolving practice and future considerations. Prostate Cancer Prostatic Dis. *22*, 24–38.
49. Hamid, A.R.A.H., Tendi, W., Sesari, S.S., Mochtar, C.A., Umbas, R., Verhaegh, G., and Schalken, J.A. (2019). The importance of targeting intracrinology in prostate cancer management. World J. Urol. *37*, 751–757.
50. Yanagisawa, T., Rajwa, P., Thibault, C., Gandaglia, G., Mori, K., Kawada, T., Fukuokaya, W., Shim, S.R., Mostafaei, H., Motlagh, R.S., et al. (2022). Androgen Receptor Signaling Inhibitors in Addition to Docetaxel with Androgen Deprivation Therapy for Metastatic Hormone-sensitive Prostate Cancer: A Systematic Review and Meta-analysis. Eur. Urol. *82*, 584–598.
51. Gheorghe, G.S., Hodorogea, A.S., Ciobanu, A., Nanea, I.T., and Gheorghe, A.C.D. (2021). Androgen Deprivation Therapy, Hypogonadism and Cardiovascular Toxicity in Men with Advanced Prostate Cancer. Curr. Oncol. *28*, 3331–3346.
52. Tagawa, S.T., Ramaswamy, K., Huang, A., Mardekian, J., Schultz, N.M., Wang, L., Sandin, R., Lechpammer, S., and George, D.J. (2021). Survival outcomes in patients with chemotherapy-naive metastatic castration-resistant prostate cancer treated with enzalutamide or abiraterone acetate. Prostate Cancer Prostatic Dis. *24*, 1032–1040.
53. Abida, W., Cyrta, J., Heller, G., Prandi, D., Armenia, J., Coleman, I., Cieslik, M., Benelli, M., Robinson, D., Van Allen, E.M., et al. (2019). Genomic correlates of clinical outcome in advanced prostate cancer. Proc. Natl. Acad. Sci. USA *116*, 11428–11436.
54. Hatano, K., and Nonomura, N. (2023). Systemic Therapies for Metastatic Castration-Resistant Prostate Cancer: An Updated Review. World J Mens Health *41*, 769–784.
55. Yin, L., Liu, Y., Peng, Y., Peng, Y., Yu, X., Gao, Y., Yuan, B., Zhu, Q., Cao, T., He, L., et al. (2018). PARP inhibitor veliparib and HDAC inhibitor SAHA synergistically co-target the UHRF1/BRCA1 DNA damage repair complex in prostate cancer cells. J. Exp. Clin. Cancer Res. *37*, 153.
56. Sheehan, B., Guo, C., Neeb, A., Paschalis, A., Sandhu, S., and de Bono, J.S. (2022). Prostate-specific Membrane Antigen Biology in Lethal Prostate Cancer and its Therapeutic Implications. Eur. Urol. Focus *8*, 1157–1168.
57. Marques, R.B., Aghai, A., de Ridder, C.M.A., Stuurman, D., Hoeben, S., Boer, A., Ellston, R.P., Barry, S.T., Davies, B.R., Trapman, J., and van Weerden, W.M. (2015). High Efficacy of Combination Therapy Using PI3K/AKT Inhibitors with Androgen Deprivation in Prostate Cancer Preclinical Models. Eur. Urol. *67*, 1177–1185.
58. Vitkin, N., Nersesian, S., Siemens, D.R., and Koti, M. (2019). The Tumor Immune Contexture of Prostate Cancer. Front. Immunol. *10*, 603.
59. Guo, Y., Tian, G., Chen, X., Hou, Y., Zhang, X., Xue, X., Zhao, L., and Wu, Y. (2023). GL-V9 ameliorates liver fibrosis by inhibiting TGF-β/smad pathway. Exp. Cell Res. *425*, 113521.
60. Chaudagar, K., Hieromnimon, H.M., Khurana, R., Labadie, B., Hirz, T., Mei, S., Hasan, R., Shafran, J., Kelley, A., Apostolov, E., et al. (2023). Reversal of Lactate and PD-1-mediated Macrophage Immunosuppression Controls Growth of PTEN/p53-deficient Prostate Cancer. Clin. Cancer Res. *29*, 1952–1968.
61. Pang, X., Zhang, J., He, X., Gu, Y., Qian, B.Z., Xie, R., Yu, W., Zhang, X., Li, T., Shi, X., et al. (2021). SPP1 Promotes Enzalutamide Resistance and Epithelial-Mesenchymal-Transition Activation in Castration-Resistant Prostate Cancer via PI3K/AKT and ERK1/2 Pathways. Oxid. Med. Cell. Longev. *2021*, 5806602.
62. Shen, T., Wang, W., Zhou, W., Coleman, I., Cai, Q., Dong, B., Ittmann, M.M., Creighton, C.J., Bian, Y., Meng, Y., et al. (2021). MAPK4 promotes prostate cancer by concerted activation of androgen receptor and AKT. J. Clin. Invest. *131*, e135465.
63. Bhatia, V., and Ateeq, B. (2019). Molecular Underpinnings Governing Genetic Complexity of ETS-Fusion-Negative Prostate Cancer. Trends Mol. Med. *25*, 1024–1038.
64. Bu, L., Wang, H., Pan, J.A., Chen, L., Xing, F., Wu, J., Li, S., and Guo, D. (2021). PTEN suppresses tumorigenesis by directly dephosphorylating Akt. Signal Transduct. Target. Ther. *6*, 262.
65. Jamaspishvili, T., Berman, D.M., Ross, A.E., Scher, H.I., De Marzo, A.M., Squire, J.A., and Lotan, T.L. (2018). Clinical implications of PTEN loss in prostate cancer. Nat. Rev. Urol. *15*, 222–234.
66. Ma, L., Yan, Y., Bai, Y., Yang, Y., Pan, Y., Gang, X., Karnes, R.J., Zhang, J., Lv, Q., Wu, Q., and Huang, H. (2019). Overcoming EZH2 Inhibitor Resistance by Taxane in PTEN-Mutated Cancer. Theranostics *9*, 5020–5034.
67. Qi, Z., Xu, Z., Zhang, L., Zou, Y., Li, J., Yan, W., Li, C., Liu, N., and Wu, H. (2022). Overcoming resistance to immune checkpoint therapy in PTEN-null prostate cancer by intermittent anti-PI3Kalpha/beta/delta treatment. Nat. Commun. *13*, 182.
68. Hu, P., Li, H., Yu, X., Liu, X., Wang, X., Qing, Y., Wang, Z., Wang, H., Zhu, M., Xu, J., et al. (2019). GL-V9 exerts anti-T cell malignancies effects via promoting lysosome-dependent AKT1 degradation and activating AKT1/FOXO3A/BIM axis. Free Radic. Biol. Med. *145*, 237–249.
69. Chan, C.H., Morrow, J.K., Li, C.F., Gao, Y., Jin, G., Moten, A., Stagg, L.J., Ladbury, J.E., Cai, Z., Xu, D., et al. (2013). Pharmacological inactivation of Skp2 SCF ubiquitin ligase restricts cancer stem cell traits and cancer progression. Cell *154*, 556–568.
70. Liu, J., Peng, Y., Shi, L., Wan, L., Inuzuka, H., Long, J., Guo, J., Zhang, J., Yuan, M., Zhang, S., et al. (2021). Skp2 dictates cell cycle-dependent metabolic oscillation between glycolysis and TCA cycle. Cell Res. *31*, 80–93.
71. Chelakkot, C., Chelakkot, V.S., Shin, Y., and Song, K. (2023). Modulating Glycolysis to Improve Cancer Therapy. Int. J. Mol. Sci. *24*, 2606.
72. Visca, P., Pisa, F., and Imperi, F. (2019). The antimetabolite 3-bromopyruvate selectively inhibits Staphylococcus aureus. Int. J. Antimicrob. Agents *53*, 449–455.
73. Vital, P.D.S., Bonatelli, M., Dias, M.P., de Salis, L.V.V., Pinto, M.T., Baltazar, F., Maria-Engler, S.S., and Pinheiro, C. (2022). 3-Bromopyruvate Suppresses the Malignant Phenotype of Vemurafenib-Resistant Melanoma Cells. Int. J. Mol. Sci. *23*, 15650.
74. Tortorella, E., Giantulli, S., Sciarra, A., and Silvestri, I. (2023). AR and PI3K/AKT in Prostate Cancer: A Tale of Two Interconnected Pathways. Int. J. Mol. Sci. *24*, 2046.
75. Masiello, D., Cheng, S., Bubley, G.J., Lu, M.L., and Balk, S.P. (2002). Bicalutamide functions as an androgen receptor antagonist by assembly of a transcriptionally inactive receptor. J. Biol. Chem. *277*, 26321–26326.
76. Liu, J., Guo, Y., Zhang, R., Xu, Y., Luo, C., Wang, R., Xu, S., and Wei, L. (2023). Inhibition of TRPV4 remodels single cell polarity and suppresses the metastasis of hepatocellular carcinoma. Cell Death Dis. *14*, 379.

CellPress
OPEN ACCESS

STAR★METHODS

KEY RESOURCES TABLE

REAGENT or RESOURCE	SOURCE	IDENTIFIER
Antibodies		
Rabbit anti-Actin	ABclonal Technology, China	AC026; RRID: AB_2768234
Rabbit anti-Caspase 3	Proteintech Group, USA	66470-2-Ig; RRID: AB_2876892
Rabbit anti-Cleaved caspase 3	ABclonal Technology, China	A11021; RRID: AB_2758369
Rabbit anti-Caspase 8	Proteintech Group, USA	66093-1-Ig; RRID: AB_11232214
Rabbit anti-Caspase 9	Proteintech Group, USA	66169-1-Ig; RRID: AB_2833257
Rabbit anti-PARP	Proteintech Group, USA	66520-1-Ig; RRID: AB_2881883
Rabbit anti-BCL2	ABclonal Technology, China	A0208; RRID: AB_2757022
Rabbit anti-BAX	ABclonal Technology, China	A19684; RRID: AB_2862733
Rabbit anti-HK2	Proteintech Group, USA	66974-1-Ig; RRID: AB_2882294
Mouse anti-LDHA	Proteintech Group, USA	66287-1-Ig; RRID: AB_2881670
Rabbit anti-PFKM	Proteintech Group, USA	55028-1-AP; RRID: AB_10858390
Rabbit anti-PKM1	Proteintech Group, USA	15821-1-AP; RRID: AB_2163820
Rabbit anti-PKM2	Proteintech Group, USA	15822-1-AP; RRID: AB_1851537
Mouse anti-AKT	Proteintech Group, USA	60203-2-Ig; RRID AB_10912803
Rabbit Phospho-AKT (Ser473)	Proteintech Group, USA	80455-1-RR; RRID: AB_2918892
Rabbit anti-AR	Proteintech Group, USA	22089-1-AP; RRID: AB_11182176
Rabbit anti-Androgen Receptor (Phospho Ser81)	Immunoway, USA	YP1861; RRID: AB_805251
Rabbit anti-COX IV	ABclonal Technology, China	A6564; RRID: AB_2767158
Rabbit anti-Cytochrome c	Proteintech Group, USA	10993-1-AP; RRID: AB_2090467
Goat anti-Rabbit IgG (H+L) Highly Cross-Adsorbed Secondary Antibody, Alexa Fluor™ Plus 488	Thermo Scientific, USA	A32731
Goat anti-Mouse IgG (H+L) Highly Cross-Adsorbed Secondary Antibody, Alexa Fluor™ Plus 555	Thermo Scientific, USA	A32727
Chemicals, peptides, and recombinant proteins		
GL-V9 (5-hydroxy-8-methoxy-7-(4-(pyrrolidin-1-yl) butoxy)-4 Hchromen-4-one, $C_{24}H_{27}NO_5$, MW 409.47, purity >99%)	Jiangsu Key Laboratory of Carcinogenesis and Intervention, China Pharmaceutical University	N/A
3-Bromopyruvic acid	Selleck Chemicals, China	S5426
Bicalutamide	Selleck Chemicals, China	S1190
MK-2206	MedChemExpress, China	1032349-77-1
SF1670	MedChemExpress, China	345630-40-2
TEPP-46	MedChemExpress, China	1221186-53-3
5-Fluorouracil	MedChemExpress, China	51-21-8
Z-IETD-FMK	MedChemExpress, China	210344-98-2
BI-6c9	MedChemExpress, China	791835-21-7
Mito-SOX Red	MedChemExpress, China	1003197-00-9
pyruvate sodium	Thermo Scientific, USA	11360070
L-Glutamine	Thermo Scientific, USA	25030081
DAPI Staining Solution	Beyotime Biotechnology	C1005
Dimethyl sulfoxide	Sigma Aldrich, USA	67-68-5

(*Continued on next page*)

Continued

REAGENT or RESOURCE	SOURCE	IDENTIFIER
Critical commercial assays		
Lactic Acid Detection kit	KeyGEN Bio TECH, China	KGT022
Amplex® Red Glucose/Glucose Oxidase Assay Kit	Thermo Scientific, USA	A22189
Pierce™ BCA Protein Assay Kits	Thermo Scientific, USA	23227
Ultra-Sensitive SP kit	Maixin Biotechnologies	kit 9710
RNA-easy Isolation Reagent	Vazyme, China	R701-01
XF Cell Mito Stress Test Kit	Agilent, USA	103010-100
XF Glycolysis Stress Test Kit	Agilent, USA	103020-100
Mitochondrial Membrane Potential Assay Kit with JC-1	Beyotime Biotechnology	C2003S
Annexin-V/PI double-staining assay	Vazyme, China	A211-01
CCK-8 Cell Counting Kit	Vazyme, China	A311-01
ATP Assay Kit	Beyotime Biotechnology	S0026
Reactive Oxygen Species Assay Kit	Beyotime Biotechnology	S0033S
Super Signal ECL	Thermo Scientific	A38554
AceQ qPCR SYBR Green Master Mix	Vazyme, China	Q131-02
HiScript II Q RT SuperMix for qPCR	Vazyme, China	R223-01
GenJet™ transfection reagent	SignaGen, USA	SL100489
Experimental models: Cell lines		
22RV1	Cell Bank of Shanghai Institute of Biochemistry & Cell Biology, China	TCHu173, CSTR:19375.09.3101HUMTCHu173
PC-3	Cell Bank of Shanghai Institute of Biochemistry & Cell Biology, China	SCSP-532, CSTR:19375.09.3101HUMSCSP532
LNCaP	Cell Bank of Shanghai Institute of Biochemistry & Cell Biology, China	TCHu173, CSTR:19375.09.3101HUMTCHu173
DU 145	Cell Bank of Shanghai Institute of Biochemistry & Cell Biology, China	SCSP-5024, CSTR:19375.09.3101HUMSCSP5024
RM-1	Cell Bank of Shanghai Institute of Biochemistry & Cell Biology, China	TCM14, CSTR:19375.09.3101MOUTCM14
Experimental models: Organisms/strains		
Male athymic nude mice	Gempharmatech Co., Ltd, China	N/A
Oligonucleotides		
GTACAGCCAGTGTGTCCGAA	Gene Denovo, China	*AR*-Forward Primer
TTGGTGAGCTGGTAGAAGCG	Gene Denovo, China	*AR*- Reverse Primer
ATGAACGACGTAGCCATTGTG	Gene Denovo, China	*AKT*- Forward Primer
TTGTAGCCAATAAAGGTGCCAT	Gene Denovo, China	*AKT*- Reverse Primer
Software and algorithms		
Prism 9.0.0	Graphpad	N/A
ImageJ	https://imagej.nih.gov	N/A
Flowjo X	http://www.flowjochina.com/	N/A
Adobe illustrator 2021	https://www.adobe.com/	N/A
National Center for Biotechnology Information	https://www.ncbi.nlm.nih.gov/	N/A

RESOURCE AVAILABILITY

Lead contact

Further information and requests for reagents and resources should be directed to and will be fulfilled by the lead contact, Libin Wei (wlbiws_1986@aliyun.com).

CellPress
OPEN ACCESS

Material availability

All materials in this study will be made available on request to the lead contact.

Data and code availability

- All data reported in this paper will be shared by the lead contact upon request.
- This paper does not report original code.
- Any additional information required to reanalyze the data reported in this paper is available from the lead contact upon request.

EXPERIMENTAL MODEL AND STUDY PARTICIPANT DETAILS

Mouse models

Male athymic nude mice (4–6 weeks old) weighing 18–22 g were purchased from the Gempharmatech Co., Ltd., Shanghai, China. All mouse experiments were in compliance with the policies of the SFDA (State Food and Drug Administration) of China on Animal Care. The experimental protocol was reviewed and approved by the Ethical Committee of China Pharmaceutical University, Nanjing, China. Animals are housed in IVC cages with adequate high-temperature sterilized water, sterile feed and regular light exposure. Room temperature was controlled at 24°C–26°C and humidity at 40–60%. Approximately 1×10^6 22RV1 or PC3 cells were suspended and injected subcutaneously into the flanks of the nude mice to induce transplanted tumors. Recorded size of subcutaneous tumors and weight of nude mice every 3 days, and randomly divided the mice with similar tumor sizes into four groups with eight individuals each.

A gavage study on the long-term toxicity in rats indicated a maximum tolerated dose (MTD) of 450 mg/kg. This was then converted to around 650 mg/kg in mice. And in our previous studies, we chose 300 mg/kg GL-V9 using in xenograft models, which showed effective anticancer effect *in vivo*.[76] Therefore, we positioned the *in vivo* research concentrations at high and low concentrations, 300 mg/kg and 150 mg/kg, respectively. The nude mice were treated with 150 mg/kg, 300 mg/kg GL-V9 (p.o.) once daily or 20 mg/kg 5-Fluorouracil (i.v.) per trid. After treatment, the nude mice were sacrificed, and the tumor xenografts were picked and measured. Collected blood samples of nude mice from eyeballs to test complete blood count and obtained serum by centrifuging blood at 3000 rpm for 15 min to test biochemical function detection.

In the studies of drug combination therapy, mice in the 22RV1 xenograft model were administrated with GL-V9 (300 mg/kg, p.o., once daily), docetaxel (10 mg/kg, p.o., once daily) or a combination of both. Mice in the PC3 xenograft model were administrated with GL-V9 (300 mg/kg, p.o., once daily), bicalutamide (20 mg/kg, p.o, once daily), or a combination of both.

To evaluate tumor growth delay, xenograft models were created using 22RV1 cells and treated with GL-V9 (300 mg/kg, p.o, once daily) and bicalutamide (20 mg/kg, p.o, once daily) either alone or in combination for 12 days. Administration was then withdrawn and the models were sacrificed on day 27.

Cell lines - 22RV1, LNCaP, PC-3, DU 145 and RM-1 were purchased from the Cell Bank of Shanghai Institute of Biochemistry & Cell Biology. All the cell lines were authenticated with short tandem repeat (STR) analysis. LNCap and 22RV1 are AR-expressing human PCa cell lines, PC3 and DU145 are AR-negative human PCa cell lines. RM-1 is a cell line with fibroblast like morphology isolated from the prostate of 17 days old mice.

METHOD DETAILS

Cell culture

Prostate cancer cell lines 22RV1, LNCaP, PC-3 and RM-1 were cultured in PRMI-1640 (GIBCO, Invitrogen) with 10% heat-inactivated fetal bovine serum (FBS, WISENT), 1% pyruvate sodium and L-Glutamine, 100 U/mL penicillin G, and 100 μg/mL streptomycin at 37°C with 5% CO_2. DU 145 cells were cultured in DMEM (GIBCO, Invitrogen) with 10% heat-inactivated FBS (WISENT), 1% pyruvate sodium and L-Glutamine, 100 U/mL penicillin G, and 100 μg/mL streptomycin at 37°C with 5% CO_2.

Cell viability and apoptosis assays

Cell viability was measured using Cell Counting Kit-8 (CCK-8). Cells (8×10^3) were treated with GL-V9 for 48 h at various concentrations (0–100 μM). Using a Universal Microplate Reader EL800 (BIO-TEK instruments, Inc.) to measure absorbance of the resulting formazan spectrophotometrically at 450 nm. Apoptosis of cells was assayed with Annexin-V/PI double-staining assay. Prostate cancer Cells were treated for 48 h with drugs, then harvested and resuspended with pre-cooled PBS without EDTA. Apoptosis of cells were identified by double supravital staining with Annexin V-FITC and PI. Apoptotic cell death was examined by FACSCalibur flow cytometry (Becton Dickinson).

Measurement of intracellular Reactive Oxygen Species (ROS) levels

Intracellular ROS levels were measured using Reactive Oxygen Species Assay Kit (Beyotime Biotechnology). The prostate cancer cells were pretreated with different concentrations of GL-V9 for 48 h. Cultured cells were washed once and incubated with DCFH-DA diluted to 10 μM with PBS for 20 min at 37°C cell culture incubator. Flow cytometry (Becton Dickinson) was used to measure the fluorescence intensity.

Measurement of mitochondrial membrane potential (MMP)

Measurement of MMP of cells was measured with Mitochondrial Membrane Potential Assay Kit with JC-1 (Beyotime Biotechnology). Cells were resuspended with JC-1 and RIPA-1640 (1:1000) and incubated for 20 min at 37°C cell culture incubator. Then cells were centrifuged (600 g × 5 min at 4°C) and abandon the supernatant. Cells were washed twice and resuspend with pre-cooled JC-1 staining buffer(1X). MMP was detected by FACSCalibur flow cytometry (Becton Dickinson, San Jose, CA).

Measurement of lactic acid production, glucose uptake and ATP generation

The level of lactic acid in the cell culture media was measured using the Lactic Acid Detection kit (KeyGEN Bio TECH). The cell culture medium of cells was collected. Lactic acid production was tested following the manufacturer's instructions by spectrophotometer (Thermo) at 530 nm. All measurements were normalized according to the number of cells in each experiment.

The glucose uptake of prostate cancer cells was measured using the Amplex Red Glucose/Glucose Oxidase Assay Kit (Invitrogen). The culture medium of each experiment was collected, and then diluted 1:2400 in water. The quantity of glucose was then detected following the manufacturer's instructions using Thermo Scientific Varioskan Flash spectral scanning multimode reader (Thermo) with an excitation range of 530–560 nm and an emission detection at 590 nm. The glucose uptake was calculated by subtracting the amount of glucose in each sample from the total amount of glucose in the media without cells. The relative glucose uptakes were normalized according to the number of cells in each experiment.

The intracellular ATP of cells was quantified using ATP Assay Kit (Beyotime Biotechnology). Cells were collected and lysed with Cell Lysis Reagent on ice. After centrifugation of the lysis at a force of 12000 g for 5 min at 4°C, the supernatant was withdrawn and used for further assays following the instructions of the manufacturer. The measurements were normalized based on the number of cells used in each experiment.

Measurement of ECAR and OCR

Cells were split into XF96 cell culture plates for the Seahorse Extracellular Flux Analyzer (Seahorse Biosciences). This provided real-time measurements of the oxygen consumption rate (OCR) as a measure of OXPHOS, and the extracellular acidification rate (ECAR) as a measure of glycolysis. Upon drug treatment, cells were treated according to Agilent Seahorse XF Cell Mito Stress Test and Glycolytic Stress Test instructions. The experimental results were analyzed by Wave software.

Briefly, 8×10^3 22RV1 or PC3 cells were seeded into each well of XF96 cell culture plates (Seahorse Bioscience) with 10% FBS RIPM-1640, then treated with tested drugs for 24 h at 37°C with 5% CO_2. The utility plate of XF96 probe plate was hydrated one day in advance with 200 μL sterile ultra-pure water (ddH_2O) in a 37°C/non-CO_2 incubator prior to renewing ddH_2O to agilent seahorse XF calibrant before the assay. One hour before the assay, to suck away RIPM1640 and gently wash twice with seahorse base medium (PH = 7.4) and eventually put into a 37°C/non-CO_2 incubator. For ECAR measured by XF Glycolysis Stress Test Kit, 10 mM glucose, 1 μM oligomycin and 50 mM 2-deoxyglucose (2-DG) were added to the A-C wells of the XF96 probe plate. For OCR measured by XF Cell Mito Stress Test Kit, 1 μM oligomycin (Oligo, port A), 1 μM Carbonyl cyanide 4-(trifluoromethoxy) phenylhydrazone (FCCP, port B), 0.5 μM rotenone and 0.5 μM antimycin A (port C) were added to the A-C wells of probe plate. The results of ECAR and OCR were detected with XF96 Extracellular Flux analyzer after calibration and all Seahorse measurements were normalized to the cell number in each well.

Gene expression studies (QPCR)

Cell cultures were washed with phosphate-buffered saline and then scaped into RNA-easy Isolation Reagent to isolate RNA according to the instructions. Reverse transcriptase reactions were carried out using 1.5 mg of RNA and the HiScript II Q RT SuperMix for qPCR (Vazyme). Real-time qPCR was carried out using AceQ qPCR SYBR Green Master Mix (Vazyme) using primer sequences obtained from PrimerBank (http://pga.mgh.harvard.edu/primerbank/index.html).

Immunofluorescence

The cells were cultured on cover glass and treated with GL-V9 for 24 h. Then the cells were washed three times for 5 min with pre-cooled PBS, fixed with 10% formaldehyde for 30 min, again washed three times with pre-cooled PBS, and then permeabilized cells with Triton X-100 for 20 min. After that, the cells were blocked at room temperature by 5% BSA for 1 h and incubated with anti-HKII antibody and TOM20 (Proteintech Group, Inc) overnight at 4°C, followed by incubation with secondary antibodies (Thermo Scientific) for 1 h at 37°C. Finally, the cells were stained with diamidino-phenyl-indole (DAPI) for 10 min. The intracellular distribution of HKII and TOM20 was observed using an FV1000 confocal laser scanning biomicroscope (Olympus).

Western blot

Cytosolic extracts, mitochondrial extracts and the whole cell lysates were prepared according to the manufacturer's protocol and quantified by the BCA Protein Assay (Thermo Fisher Scientific). Separated protein samples (40 μg/sample) using SDS-PAGE and transferred them into the nitrocellulose (NC) membrane, then blocked membranes with 5% dried skimmed milk in PBST for 1 h prior to incubate primary antibody overnight at 4°C. Followed to incubate HRP-conjugated secondary antibodies on shock bed for 1 h at room temperature. Anti-rabbit IgG HRP

and anti-mouse IgG HRP were purchased from Abclonal Technology. Antibody conjugates were captured by chemiluminescence (ECL, Thermo Fisher Scientific).

Immunohistochemistry (IHC)

The expressions of AR, cleaved-caspase3, AKT and HKII in the tumor tissue were assessed by IHC using a rabbit antihuman monoclonal antibody and an Ultra-Sensitive SP kit (kit 9710 MAIXIN, Maixin-Bio Co.). Briefly, tumor tissue sections from various groups of mice were dewaxed at 1 h in a 60°C oven. Sections were deparaffinized and rehydrated, followed to restore antigen by boiled in citrate buffer at high temperature, and blocked endogenous peroxidase activity with 3% hydrogen peroxide. Incubated sections with 5% BSA prior to incubate the primary antibody at 4°C overnight. Then incubated with the secondary biotinylated anti-species antibody and labeled using a modified staining procedure based on avidin–biotin complex immunoperoxidase following the instructions of the Ultra-Sensitive SP kit.

Ethics

Animals were treated according to the guidelines of the National Institute of Health (publication No. 85–23, revised 1996). Animal protocols were reviewed and approved by the Ethical Committee of China Pharmaceutical University (ethical approval number CPU-2023-0303).

QUANTIFICATION AND STATISTICAL ANALYSIS

All experiments were performed at least three times. All data were analyzed using GraphPad Prism 8.0 (GraphPad, San Diego, CA, USA) and shown as means $\pm$ SD. Continuous data differences analysis was evaluated by Student's *t* test between two groups. One-way analysis of variance (ANOVA) test was used to analyze differences among multiple groups. The p value lower than 0.05 was assigned for statistically significant. Statistical details for each experiment are included in the figures and figure legends.